Atmos. Chem. Phys., 15, 12705–12729, 2015
www.atmos-chem-phys.net/15/12705/2015/
doi:10.5194/acp-15-12705-2015


Atmospheric Chemistry and Physics Open Access EGU

# Estimation of continuous anthropogenic $CO_2$: model-based evaluation of $CO_2$, CO, $\delta^{13}C(CO_2)$ and $\Delta^{14}C(CO_2)$ tracer methods

**S. N. Vardag[1], C. Gerbig[2], G. Janssens-Maenhout[3], and I. Levin[1]**

[1]Institut für Umweltphysik, Heidelberg University, Germany
[2]Max Planck Institute for Biogeochemistry, Hans-Knöll-Str. 10, 07745 Jena, Germany
[3]European Commission, Joint Research Centre, Ispra, Via Fermi 2749, 21027 Ispra, Italy

*Correspondence to:* S. N. Vardag (svardag@iup.uni-heidelberg.de)

Received: 3 July 2015 – Published in Atmos. Chem. Phys. Discuss.: 24 July 2015
Revised: 27 October 2015 – Accepted: 30 October 2015 – Published: 16 November 2015

**Abstract.** We investigate different methods for estimating anthropogenic $CO_2$ using modeled continuous atmospheric concentrations of $CO_2$ alone, as well as $CO_2$ in combination with the surrogate tracers CO, $\delta^{13}C(CO_2)$ and $\Delta^{14}C(CO_2)$. These methods are applied at three hypothetical stations representing rural, urban and polluted conditions. We find that, independent of the tracer used, an observation-based estimate of continuous anthropogenic $CO_2$ is not yet feasible at rural measurement sites due to the low signal-to-noise ratio of anthropogenic $CO_2$ estimates at such settings. The tracers $\delta^{13}C(CO_2)$ and CO provide an accurate possibility to determine anthropogenic $CO_2$ continuously, only if all $CO_2$ sources in the catchment area are well characterized or calibrated with respect to their isotopic signature and CO to anthropogenic $CO_2$ ratio. We test different calibration strategies for the mean isotopic signature and CO to $CO_2$ ratio using precise $\Delta^{14}C(CO_2)$ measurements on monthly integrated as well as on grab samples. For $\delta^{13}C(CO_2)$, a calibration with annually averaged $^{14}C(CO_2)$ grab samples is most promising, since integrated sampling introduces large biases into anthropogenic $CO_2$ estimates. For CO, these biases are smaller. The precision of continuous anthropogenic $CO_2$ determination using $\delta^{13}C(CO_2)$ depends on measurement precision of $\delta^{13}C(CO_2)$ and $CO_2$, while the CO method is mainly limited by the variation in natural CO sources and sinks. At present, continuous anthropogenic $CO_2$ could be determined using the tracers $\delta^{13}C(CO_2)$ and/or CO with a precision of about 30 %, a mean bias of about 10 % and without significant diurnal discrepancies. Hypothetical future measurements of continuous $\Delta^{14}C(CO_2)$ with a precision of 5 ‰ are promising for anthropogenic $CO_2$ determination (precision ca. 10–20 %) but are not yet available. The investigated tracer-based approaches open the door to improving, validating and reducing biases of highly resolved emission inventories using atmospheric observation and regional modeling.

## 1 Introduction

Earth's carbon budget is strongly influenced by anthropogenic $CO_2$ emissions into the atmosphere (Keeling et al., 1996; Le Quéré et al., 2015). In order to support studies of the carbon cycle and to determine net and gross carbon fluxes quantitatively, various measurement sites monitor the atmospheric $CO_2$ mole fraction worldwide. In top-down approaches and in conjunction with atmospheric transport models, these $CO_2$ measurements are used to infer total $CO_2$ emissions (Bousquet et al., 2000; Gurney et al., 2002; Peylin et al., 2013), but a differentiation into biogenic, oceanic and anthropogenic $CO_2$ sources and sinks is not feasible with $CO_2$ concentration measurements alone. Inverse model studies commonly utilize anthropogenic $CO_2$ emission inventories to estimate anthropogenic $CO_2$ and are then able to separate anthropogenic from biogenic or oceanic carbon sink and source influences. However, currently available emission inventories exhibit large discrepancies between each other of about 10–40 % at the country level (Peylin et al., 2011), and increase further with decreasing spatial scale (Gurney et al., 2005). These discrepancies suggest that biases may be on the order of about 70–100 % for highly resolved ($0.1^\circ \times 0.1^\circ$) data sets and uncertainties ($1\sigma$) of emission inventories may be between 30 and 150 % (Wang et al., 2013). In order to

better study and quantify the biospheric carbon fluxes, their underlying processes and potential feedbacks, it is desirable to reduce the current uncertainties as well as biases of emission inventories. Validation and improvement of emission inventories requires accurate and precise anthropogenic $CO_2$ estimates (as well as accurate and precise transport models) on all relevant timescales ranging from hours to years. We hereafter refer to anthropogenic $CO_2$ as fuel $CO_2$ and include non-combustion emissions such as emissions from cement industry or non-energy use of fuels as well as agricultural waste burning. Fossil fuel $CO_2$ excludes all contributions from biofuel emissions or from agricultural waste burning. We define biofuel $CO_2$ as non-fossil fuel $CO_2$ released during combustion, including solid (e.g., wood, waste, charcoal, municipal renewable waste, bagasse, vegetal waste and dung), liquid (e.g., biodiesel, bio gasoline and black liquor) and gaseous (from compost or cattle farm) biomaterial. It does not include large-scale biomass burning. For some purposes, e.g., when validating fossil fuel emission reductions, it may actually be advantageous to estimate only the fossil fuel $CO_2$ contribution, which is the fuel $CO_2$ contribution without biofuel $CO_2$. However, when solving for biospheric fluxes, the biofuel $CO_2$ is important as well, since it equally contributes to the instantaneously measured $CO_2$ concentration and needs to be separated from the biospheric flux. In the following, we seek to constrain the fuel $CO_2$ (fossil fuel $CO_2$ plus biofuel $CO_2$).

$^{14}C$ measurements are commonly used as surrogate to differentiate between biogenic and fossil fuel $CO_2$ contributions in the atmosphere, since fossil fuels do not contain any $^{14}C$, in contrast to biogenic sources (Levin et al., 2003). The $^{14}C\,/\,C$ isotope ratio in $CO_2$ is expressed on the $\Delta^{14}C(CO_2)$ scale, which denotes the deviation of the $^{14}C\,/\,C$ ratio in $CO_2$ from a standard material in per mill (Stuiver and Polach, 1977). We use the depletion of $\Delta^{14}C(CO_2)$ at a polluted measurement site relative to $\Delta^{14}C(CO_2)$ in clean background air to derive quantitative information on the contribution of fossil fuel $CO_2$ to total measured $CO_2$ mole fraction at the polluted site. Radiocarbon ($^{14}C$) is thus used as quantitative tracer for fossil fuel contributions (e.g., Levin et al., 2003; Levin and Karstens, 2007; Turnbull et al., 2006, 2015; Newman et al., 2015). However, there are a number of problems when using $^{14}C(CO_2)$ as a tracer for anthropogenic emissions. First, precise $\Delta^{14}C(CO_2)$ measurements from conventional counting or accelerator mass spectrometry (AMS; see list of all abbreviations in Appendix D) (better than 2 ‰) are time and cost intensive, thus currently prohibiting the coverage of large periods and large area of such measurements. Attempts have been made to sample $^{14}C(CO_2)$ with a higher measurement frequency using gas chromatography (GC) coupled to continuous-flow AMS (McIntyre et al., 2013), but the technique is not applicable to atmospheric $^{14}C$ samples so far and the precision in $\Delta^{14}C(CO_2)$ is lower than for AMS or conventional counting. This results in less precise fossil fuel $CO_2$ estimates. These studies indicate, however, that the measurement precision using GC and continuous-flow AMS may reach 5 ‰ in future. The benefit of such hypothetical quasi-continuous but reduced precision fossil fuel $CO_2$ estimates is assessed for the first time in this work in order to check whether these measurements would provide beneficial constraints for determining $CO_2$ continuously.

Second, a complication of applying $\Delta^{14}C(CO_2)$ measurements for fossil fuel $CO_2$ estimation is that nuclear power plants as well as nuclear fuel reprocessing plants emit $^{14}C(CO_2)$ and can bias regional $\Delta^{14}C(CO_2)$-based estimates of fossil fuel contributions if not taken into account (Levin et al., 2003; Graven and Gruber, 2011; Vogel et al., 2013b). Moreover, biofuel $CO_2$ contributions cannot be monitored with $\Delta^{14}C(CO_2)$ measurements, since they have a similar $\Delta^{14}C(CO_2)$ signature as the biosphere or may even be elevated in $^{14}C$ due to the bomb radiocarbon $^{14}C(CO_2)$ stored in wood material. This could become especially problematic, since the use of biofuels is expected to play an increasingly important role for the energy supply in the near future (Coyle, 2007). With these shortcomings of $\Delta^{14}C(CO_2)$ as a tracer for anthropogenic $CO_2$ recognized, it is worth considering other tracers for the estimation of fuel $CO_2$ contributions.

Turnbull et al. (2015) showed that for an urban study area in the middle of the North American continent, the local $CO_2$ offset relative to clean air, $\Delta CO_2$, can be used as a tracer for fuel $CO_2$ contributions if all other $CO_2$ sources and sinks, such as from the living biosphere, are negligible. This may be the case for wintertime periods in urban areas when using a background station upwind and close to the urban area. However, we do not expect $\Delta CO_2$ to be a quantitative tracer when biospheric fluxes occur within the study area. This is normally the case in spring, summer and autumn.

Since CO is often co-emitted during (incomplete) combustion and since CO can be measured continuously, the CO offset relative to clean air, $\Delta CO$, is frequently used as a tracer for fuel $CO_2$ (Meijer et al., 1996; Gamnitzer et al., 2006; Rivier et al., 2006; Turnbull et al., 2006, 2011; Levin and Karstens, 2007; Vogel et al., 2010; Newman et al., 2013). If the mean ratio of the CO offset ($\Delta x$) relative to the fuel $CO_2$ offset ($\Delta y_F$), i.e., $\Delta x/\Delta y_F \equiv \overline{R_F}$, is known and relatively constant within 1 month, it is principally possible to derive a continuous $\Delta y_F$ estimate from $\Delta x$ measurements by dividing $\Delta x$ by monthly mean $\overline{R_F}$. The overbar is used to emphasize that we use one averaged value for $R_F$, even though it actually varies with the relative fraction of the different emission groups in a varying catchment area of the measurement site. CO is also produced during oxidation of methane and hydrocarbons, particularly during summer (Granier et al., 2000). The main sinks of CO are photooxidation and reaction with OH (Parrish et al., 1993) as well as soil uptake (Inman et al., 1971), leading to a rather short atmospheric lifetime of CO of several weeks in summer (Prather et al., 2001). Natural CO sinks and sources vary on timescales of hours to seasons. Further, relative contributions of different fuel

$CO_2$ sectors (e.g., energy production, road traffic, residential heating, industrial emissions) with different emission ratios ($\Delta CO / \Delta CO_2$) may vary on short timescales of hours to longer timescales of years if, for example, combustion technologies, processes and procedures change in the long term. Therefore, the mean $\overline{R_F}$ ($= \Delta x / \Delta y_F$) is a function of space and time and might need to be calibrated using, for example, $\Delta^{14}C(CO_2)$ measurements (Levin and Karstens, 2007). If $\overline{R_F}$ does not vary significantly within the timescale of the calibration, continuous $\Delta y_F$ can be estimated. However, if $\overline{R_F}$ varies strongly on timescales of smaller than the calibration interval, further corrections (e.g., diurnal or seasonal) may be necessary (Vogel et al., 2010). These corrections are only reliable if $\overline{R_F}$ variations are systematic. Since this is not always the case, additional or other continuous tracers may need to be considered to improve fuel $CO_2$ estimates.

One of these tracers may be $\delta^{13}C(CO_2)$, since fuel emissions tend to be more depleted in $^{13}CO_2$ than fluxes from the biosphere. Zondervan and Meijer (1996), Pataki et al. (2006) and Djuricin et al. (2010) attempted to estimate fuel $CO_2$ emissions in specific case studies using mass spectrometric measurements of $\delta^{13}C(CO_2)$, in addition to $\Delta^{14}C(CO_2)$ measurements. Recently, new optical instrumentation allows for $\delta^{13}C(CO_2)$ to be measured continuously (e.g., Esler et al., 2000; Tuzson et al., 2011; Hammer et al., 2013; Vogel et al., 2013a), thus opening the door for $\delta^{13}C(CO_2)$ as a continuous tracer for fuel $CO_2$ contributions. In order to use $\delta^{13}C(CO_2)$ measurements at an urban site, the mean isotopic signature of the sources (and sinks) in the catchment area of the site, $\overline{\delta_F}$, must be known (Newman et al., 2015) and relatively constant and potentially require calibration (as discussed for CO). Further, the signature of fuel $CO_2$ emissions must be significantly different from biospheric $CO_2$ emissions in order to differentiate properly between them.

In many settings, we will exhibit neither a constant ratio $\overline{R_F}$ nor a constant fuel source signature $\overline{\delta_F}$. This will especially be the case if multiple sources (i) with different emission ratios $R_{F,i}$ and from different fuel $\delta^{13}C(CO_2)$ source signatures $\delta_{F,i}$ are located in the catchment area of the measurement site. In these cases, it may be advantageous to divide the fuel emissions into (two) different groups. CO will only be an adequate tracer for a certain emission group if this group has a significantly different ratio $\overline{R_F}$ ($= \Delta x / \Delta y_F$) than any other emission group. By analogy, $\delta^{13}C(CO_2)$ will only be a good tracer for a certain emission group if the group's emissions are significantly more depleted or enriched with respect to the other groups. If we divide all fuel $CO_2$ contributions into two emission groups, of which one is well constrained by CO and the other by $\delta^{13}C(CO_2)$, we may then join both tracers to determine the total fuel $CO_2$ contributions. In several published studies, the CO mole fraction has been used as a tracer for traffic emissions only (e.g., Schmidt et al., 2014), since these often exhibit high $\Delta CO / \Delta CO_2$ ratios. However, in some regions, emission inventories (e.g., Landesamt für Umwelt, Messungen und Naturschutz Baden-Württemberg, available at http://www.ekat.baden-wuerttemberg.de/) show that the emission ratio $\overline{R_{tr}}$ ($= (\Delta x / \Delta y)_{tr}$) has been decreasing during the last decade, degrading CO as a tracer for traffic contributions. At the same time, diesel/gasoline for vehicles is blended with an increasing amount of biodiesel/biogasoline (on the order of 5 % for OECD countries; IEA, 2014). More in general, emission inventories show that (the sum of solid, liquid and gaseous) biofuel $CO_2$ emissions in OECD countries have increased (IEA, 2014) and that the mean emission ratio of biofuel emissions $\overline{R_{bf}}$ ($= (\Delta x / \Delta y)_{bf}$) is very high (EDGARv4.3 emission inventory; EC-JRC/PBL, 2015), qualifying CO as a tracer for biofuel contributions. However, the emission ratio varies depending on the combustion type. Later we examine separately whether these two emission groups, traffic and biofuel emissions, could possibly be traced with CO.

In the present study, we investigate how continuous $CO_2$, CO, $\delta^{13}C(CO_2)$ and $\Delta^{14}C(CO_2)$ measurements as well as the combination of these tracers could be used to estimate continuous fuel $CO_2$. In order to validate how precisely and accurately we may be able to determine fuel $CO_2$ using continuous (hourly) $CO_2$, CO, $\delta^{13}C(CO_2)$ and $\Delta^{14}C(CO_2)$ as tracers, we use a modeled data set, in which, contrary to measured data sets, $CO_2$ contributions from all source categories, i.e., the biosphere, from fossil fuel and from biofuel burning are traced separately. Using the modeled mole fractions and isotope records of $CO_2$, CO, $\delta^{13}C(CO_2)$ and $\Delta^{14}C(CO_2)$, we estimate the total fuel $CO_2$ offset using these tracers. We then discuss advantages and disadvantages of the different tracers. Using a modeled data set has the additional advantage that isotopic signatures, emission ratios of different emission sectors etc. can be varied in order to also investigate the sensitivity of these source characteristics on the fuel $CO_2$ estimate. This enables us to judge how accurately the sources in the catchment of the measurement site need to be characterized for a certain required accuracy of fuel $CO_2$, and if a calibration, using, for example, precise $\Delta^{14}C(CO_2)$ measurements, is advantageous. In the course of this, we also compare different possible sampling strategies for calibration. We further assess which measurement precision is needed to achieve continuous fuel $CO_2$ estimates with sufficient precision. Additionally, we investigate the diurnal cycle of the tracer-based continuous fuel $CO_2$ estimates and compare them to the modeled reference fuel $CO_2$ in order to determine whether we can reproduce the diurnal cycle correctly and hence whether we would introduce significant biases when using, for example, only afternoon values of fuel $CO_2$ in inverse models.

We discuss the model results for three typical European sites, which differ in their annual mean fuel $CO_2$ offset. We define three pollution regimes, which we call "rural", "urban" and "polluted". Rural sites have mean fuel $CO_2$ offsets of 0–5 µmol mol$^{-1}$. We here use the (hypothetical) station Gartow (53°0′ N, 11°3′ E) as an example with an annual

mean fuel $CO_2$ offset of 3 µmol mol$^{-1}$. Gartow is located in northern Germany about 160 km northwest of Berlin. Urban sites span a range from 5 to 20 µmol mol$^{-1}$. We use Heidelberg (49°3′ N, 8°4′ E) as an example, which is a typical urban measurement site with large fuel $CO_2$ emissions but also similarly high biogenic sources and sinks in the catchment, which are also active during relatively mild winters. The mean modeled fuel $CO_2$ offset in Heidelberg is about 16 µmol mol$^{-1}$ (24 h). Polluted sites exhibit annual mean fuel $CO_2$ offsets larger than 20 µmol mol$^{-1}$. A station in the outskirts of Berlin (52°5′ N, 13°6′ E) is used as an example site with modeled mean fuel $CO_2$ offset of 25 µmol mol$^{-1}$. For all sites, we looked at the same height above ground level (30 m a.g.l). Note that this classification relates only to the mean annual offset and not to single pollution events. We assess whether an estimation of continuous fuel $CO_2$ is possible at all sites and what may be the best tracer. Finally, we give an outlook on how to apply this model study to a real measured data set. Our investigation aims at providing the basis for the decision of whether it is worthwhile conducting continuous measurements of $CO_2$, CO, $\delta^{13}C(CO_2)$ and $\Delta^{14}C(CO_2)$ at a particular measurement station in order to quantitatively and precisely estimate continuous fuel $CO_2$ within a measurement network.

## 2 The modeling framework

For the study's purpose of theoretically assessing precision and accuracy of different tracer configurations for fuel $CO_2$ estimation, it is only of secondary importance that modeled time series be correct, but it is mainly important that the model provides a reasonably realistic data set. In this study, we simulate mole fractions and isotopic records for the Heidelberg site (urban; see Levin et al., 2003) and for two hypothetical stations Gartow (rural) and Berlin (polluted) for the year 2012. All three stations may potentially be part of the German ICOS atmospheric network (see http://www.icos-infrastructure.eu/).

We used the Stochastic Time-Inverted Lagrangian Transport (STILT) model (Lin et al., 2003) as well as preset source and sink distributions (see below). To simulate the atmospheric transport we used meteorological fields from the European Centre for Medium-Range Weather Forecast with 3-hourly temporal resolution and 25 km × 25 km spatial resolution (Trusilova et al., 2010). Details of the STILT model are given in Lin et al. (2003) and in Gerbig et al. (2003); here we only provide a few relevant details. By emitting 100 particles (representing the observed air parcel) at the measurement location and inverting the meteorological fields in time, it is possible to follow the particles' trajectories backward in time using mean wind and a parameterization for the turbulent motion. For each of the trajectories, the sensitivity to emission fluxes is derived based on the residence time within the lower half of the mixed layer during each advection time step (typically 0.25 to 1 h). The sensitivity of the observed tracer mole fraction to upstream emissions was derived by combining the sensitivities of each trajectory on a common horizontal grid (here $1/12°$ latitude × $1/8°$ longitude, corresponding to about 10 km × 10 km). To reduce impact from undersampling of upstream areas at times when particles are distributed over extensive areas with large gaps between neighboring particles, the effective horizontal size of the grid cells is increased dynamically with increasing separation of the particles (Gerbig et al., 2003). This allows efficient simulations with a relatively small ensemble size. The sensitivity of the mole fraction at the measurement site to emissions located upstream is typically called the footprint. The particles are traced back in time until they leave the model domain, which extends from 16° W to 36° E and from 32 to 74° N. Initial/lateral $CO_2$ tracer boundary conditions for $CO_2$ tracer far-field mole fractions are taken from analyzed $CO_2$ fields, generated by the global atmospheric tracer transport model, TM3 (Heimann and Körner, 2003), based on optimized fluxes (Rödenbeck, 2005) transported at a spatial resolution of 4° × 5° with 19 vertical levels and a temporal resolution of 6 h (s96 v3.6, http://www.bgc-jena.mpg.de/~christian.roedenbeck/download-CO2-3D/). The footprint is multiplied by the biospheric and anthropogenic surface emissions to estimate the mole fraction change at the measurement site.

For the biospheric $CO_2$ fluxes, we use the vegetation photosynthesis and respiration model (VPRM; Mahadevan et al., 2008). The Net Ecosystem Exchange is calculated for different biome types based on SYNMAP (Jung et al., 2006) using land surface water index and enhanced vegetation index from MODIS (http://modis.gsfc.nasa.gov/) satellite data, as well as air temperature and shortwave radiation from ECMWF. VPRM results are computed at $1/12° \times 1/8°$ resolution with hourly resolution. We neglect biospheric CO and $CH_4$ fluxes in the model. CO destruction by OH and CO production via $CH_4$ oxidation is taken into account (Gerbig et al., 2003). However, CO production via non-methane hydrocarbon (NMHC) oxidation and CO uptake by soils (Conrad, 1996) are not included in the model. When using CO as a tracer for fuel $CO_2$, neglecting natural CO sources and sinks may be problematic since natural sources would lead to an overestimation and natural sinks to an underestimation of fuel $CO_2$. We will discuss this in more detail in Sects. 3.3.2 and 3.4.

Anthropogenic emissions of $CO_2$, CO and $CH_4$ are from a preliminary version of the EDGARv4.3 emission inventory (EC-JRC/PBL, 2015) which was also used for the UNEP Emissions Gap Report (Rogelj et al., 2014) for the base year 2010 and has a spatial resolution of $0.1° \times 0.1°$. The emissions are further separated following IPCC emission categories, which are again separated into fuel types (i.e., hard coal, brown coal, oil, natural gas, derived gas, biofuels etc.). To extrapolate the emissions to the year 2012 specifically we follow the approach taken

in the COFFEE data set ($CO_2$ release and Oxygen uptake from Fossil Fuel Emission Estimate) (Steinbach et al., 2011) and use specific temporal factors (seasonal, weekly and daily cycles) (Denier van der Gon et al., 2011) for different emission categories, and apply country and fuel type specific year-to-year changes at national level taken from the BP statistical review of World Energy 2014 (available at http://www.bp.com/en/global/corporate/about-bp/energy-economics/statistical-review-of-world-energy.html).

The STILT model calculates the total trace gas mole fraction of $CO_2$ ($y_{tot}$) at the measurement site as the sum of a background mole fraction $y_{bg}$, contributions from the biosphere $y_{bio}$, from different fossil fuel types $y_{ff,i}$ and different biofuel types $y_{bf,j}$:

$$y_{tot} = y_{bg} + y_{bio} + \sum_i y_{ff,i} + \sum_j y_{bf,j}. \quad (1)$$

The last two terms of Eq. (1) form the total fuel $CO_2$ ($y_F$). We can associate a total isotopic $\delta^{13}C(CO_2)$ ($\delta_{tot}$) record to the total $CO_2$ record following Mook (2001):

$$\delta_{tot} y_{tot} \approx \delta_{bg} y_{bg} + \delta_{bio} y_{bio} + \sum_i \delta_{ff,i}\, y_{ff,i} + \sum_j \delta_{bf,j}\, y_{bf,j}. \quad (2)$$

The isotopic signatures attributed to the different emission types, e.g., $\delta_{ff,i}$ and $\delta_{bio}$, are listed in Table 1. Note that we do not implement a diurnal cycle into the biospheric signature.

The total CO mole fraction ($x_{tot}$) can be balanced in analogy to $CO_2$, but we neglect biospheric CO contributions as they are expected to be small:

$$x_{tot} = x'_{bg} + \sum_i x_{ff,i} + \sum_j x_{bf,j} = x'_{bg} + \sum_i \frac{y_{ff,i}}{\overline{R_{ff,i}}} + \sum_j \frac{y_{bf,j}}{\overline{R_{bf,i}}}. \quad (3)$$

The emission ratios $\overline{R_{ff,i}}$ ($= (\Delta x/\Delta y)_{ff,i}$) depend on the emission category as well as fuel type and are determined by the emission characteristics (implied emission factors) given in EDGARv4.3. The footprint-weighted mean ratios, e.g., $\overline{R_F}$, are listed in Table A1 for Heidelberg. For the background values $\Delta^{14}C_{bg}$, $y_{bg}$, $\delta_{bg}$ and $x'_{bg}$, we use those mole fractions where $CH_4$ mole fraction reaches a minimum value within 2 days. This is mainly the case in the afternoon, when vertical mixing is strongest (for more details on the choice of background, see Appendix A2). Note that the CO background $x'_{bg}$ is denoted with a prime, since it has been corrected for chemical reactions with OH (sink) and for production from oxidation of $CH_4$ by applying a first-order chemical reaction on hourly OH and $CH_4$ fields. The contributions of fossil fuel and biofuel CO are, however, not corrected for these chemical reactions in the model, since the CO which is released in the footprint area of the measurement site typically travels only a fraction of its actual lifetime until arriving at the measurement site.

**Table 1.** $\delta^{13}C(CO_2)$ source signature of fuel types and biosphere as used in the model. The isotopic signature of the biosphere follows the findings of Ballantyne et al. (2011) for Europe. The assigned isotopic fuel values were chosen from mean measured isotopic signatures in Heidelberg (Kaul, 2007, and unpublished data) or, if not available, are similar to isotopic $\delta^{13}C(CO_2)$ values reported in Andres et al. (1994) or (for biogas) Widory et al. (2012).

| Emission source | $\delta_{ff,i}\,\delta_{bf,j}$ or $\delta_{bio}$ [‰] |
|---|---|
| Hard coal | −27 |
| Brown coal | −29 |
| Peat | −30 |
| Solid waste | −30 |
| Heavy oil | −31 |
| Light oil | −31 |
| Natural gas | −48 |
| Derived gas | −30 |
| Solid biomass | −29 |
| Bioliquid | −31 |
| Biosphere | |
| Jan | −27 |
| Feb | −26 |
| Mar | −25 |
| Apr | −24 |
| May | −23 |
| Jun | −22 |
| Jul | −22 |
| Aug | −23 |
| Sep | −24 |
| Oct | −25 |
| Nov | −26 |
| Dec | −27 |

The $\Delta^{14}C(CO_2)$ ($\Delta^{14}C_{tot}$) balance is also simulated and follows

$$y_{tot}\left(\Delta^{14}C_{tot}+1\right) \approx y_{bg}\left(\Delta^{14}C_{bg}+1\right) + y_{bio}\left(\Delta^{14}C_{bio}+1\right) + \sum_i y_{ff,i}\left(\Delta^{14}C_{ff,i}+1\right) + \sum_j y_{bf,j}(\Delta^{14}C_{bf,j}+1), \quad (4)$$

with $\Delta^{14}C_{bio}$, $\Delta^{14}C_{bf,j}$ and $\Delta^{14}C_{ff,i}$ listed in Table A1 and $CO_2$ mole fractions taken from model results. As all fossil fuel $CO_2$ sources are devoid of $^{14}C(CO_2)$, fuel $CO_2$ contributions are separated into fossil fuel and biofuel contributions.

In the following, we use six different tracers or tracer combinations to derive continuous fuel $CO_2$: (a) $CO_2$-only, (b) CO, (c) CO as a tracer for traffic and $\delta^{13}C$ as a tracer for all fuel $CO_2$ except that of traffic, (d) CO as a tracer for biofuel $CO_2$ and $\delta^{13}C(CO_2)$ as a tracer for fossil fuel $CO_2$, (e) $\delta^{13}C(CO_2)$ and (f) $\Delta^{14}C(CO_2)$. The six tracer combinations were qualitatively motivated and described in the Introduction and the equations are derived in Appendix A1 and are summarized in Table 2. They are briefly specified here with

**Table 2.** Tracer or tracer combinations, required parameters and formula for estimation of targeted fuel $CO_2$ concentration. In cases (c) and (d) we further divide fuel $CO_2$ into traffic $CO_2$ and non-traffic $CO_2$, or fossil fuel $CO_2$ and biofuel $CO_2$, respectively. In case (f) we can only estimate fossil fuel $CO_2$ with $\Delta^{14}C(CO_2)$and therefore lack biofuel $CO_2$ for a comprehensive fuel $CO_2$ estimate.

| Case | Required parameters | Formula (for derivation see Appendix A1) |
|---|---|---|
| (a) $CO_2$ | | $y_F = \Delta y$ |
| (b) CO | $\overline{R_F}$ | $y_F = \frac{\Delta x}{\overline{R_F}}$ |
| (c) CO (tr) $+\delta^{13}$C-$CO_2$ | $\overline{R_{tr}}, \overline{m_{tr}}$, $\overline{\delta_{tr}}, \overline{\delta_{F\text{-}tr}}$ | $y_F = \frac{\Delta x(t)\cdot\overline{m_{tr}}}{\overline{R_{tr}}} + \frac{y_{tot}\delta_{tot} - y_{bg}\delta_{bg} - (y_{tot}-y_{bg}-y_{bf})\delta_{bio} - y_{tr}\overline{\delta_{tr}}}{\overline{\delta_{F\text{-}tr}} - \delta_{bio}} y_{tot}$ |
| (d) CO (bf) $+\delta^{13}$C-$CO_2$ | $\overline{R_{bf}}, \overline{m_{bf}}$ $\overline{\delta_{bf}}, \overline{\delta_{ff}}$ | $y_F = \frac{\Delta x(t)\cdot\overline{m_{bf}}}{\overline{R_{bf}}} + \frac{y_{tot}\delta_{tot} - y_{bg}\delta_{bg} - (y_{tot}-y_{bg}-y_{tr})\delta_{bio} - y_{bf}\overline{\delta_{bf}}}{\overline{\delta_{ff}} - \delta_{bio}} y_{tot}$ |
| (e) $\delta^{13}$C-$CO_2$ | $\overline{\delta_F}$ | $y_F = \frac{y_{tot}\delta_{tot} - y_{bg}\delta_{bg} - (y_{tot}-y_{bg})\delta_{bio}}{\overline{\delta_F} - \delta_{bio}} y_{tot}$ |
| (f) $\Delta^{14}$C-$CO_2$ | $\Delta^{14}C_{bf}$, $\Delta^{14}C_{bio}$ | $y_F \approx y_{ff} = \frac{y_{bg}\left(\Delta^{14}C_{bg} - \Delta^{14}C_{bio}\right) - y_{tot}\left(\Delta^{14}C_{tot} - \Delta^{14}C_{bio}\right) - y_{bf}\left(\Delta^{14}C_{bio} - \Delta^{14}C_{bf}\right)}{\Delta^{14}C_{bio} + 1}$ |

their underlying assumptions. When using $CO_2$ as a tracer for anthropogenic $CO_2$ (case a in Table 2), we assume that all $CO_2$ stems from anthropogenic sources and no biospheric sources or sinks exist in the catchment area. In the CO-based method (case b in Table 2), we use CO as a tracer for anthropogenic $CO_2$ as CO is co-emitted during incomplete combustion. We assume to know the monthly mean ratio of fuel $CO_2$ to CO. In the $\delta^{13}C(CO_2)$ approach (case e in Table 2), we use the isotopic depletion of fuel $CO_2$ relative to biospheric $CO_2$ and assume to know the mean isotopic signature of fuel and biospheric $CO_2$. The $\Delta^{14}C(CO_2)$-based approach (case f in Table 2) makes use of the fact that fossil fuel $CO_2$ contains no $^{14}C(CO_2)$, in contrast to biospheric (and biofuel) $\Delta^{14}C(CO_2)$. Both need to be known for calculation. We also investigate the combination of CO and $\delta^{13}C(CO_2)$, with CO as a tracer for (1) traffic $CO_2$ (case c in Table 2) and (2) biofuel $CO_2$ and $\delta^{13}C(CO_2)$ for the respective remaining fuel $CO_2$ (case d in Table 2). This separation was made since in Europe traffic and biofuel emissions both show a rather large ratio of $CO / CO_2$ compared to emissions from other sectors, which makes CO a suitable tracer for these sectors. When separating between traffic and non-traffic fuel $CO_2$, we need to know the monthly mean values for $\overline{R_{tr}}$, $\overline{m_{tr}}$, $\overline{\delta_{tr}}$ and $\overline{\delta_{F\text{-}tr}}$. This holds equally true for separation between fossil fuel and biofuel $CO_2$. The different targeted emission groups (fuel $CO_2$, fossil fuel $CO_2$, fuel $CO_2$ without traffic, traffic $CO_2$, biofuel $CO_2$ and biospheric $CO_2$) are also listed and characterized in Table A1.

## 3 Results

We investigated how well the different tracer combinations perform at a typical urban, rural and polluted measurement site. First, we will discuss the upper limit of precision and accuracy of fuel $CO_2$ estimation using these tracers when assuming all parameters (e.g., $\overline{\delta_F}$) are known at every time step. Here, the smallest possible time step is hours. We then investigate how the use of averaged accurate parameters and variables affects the fuel $CO_2$ estimate. Next, we also perform a sensitivity analysis to identify which parameters and variables need to be known at which precision and accuracy for fuel $CO_2$ estimation with satisfying accuracy (of, for example, better than 10 %). Finally, we discuss the diurnal variation in fuel $CO_2$ and include a realistic measurement uncertainty into our considerations.

### 3.1 High (hourly) resolution of parameters and variables

The integrated footprint-weighted parameters (e.g., $\overline{R_F}$, $\overline{R_{tr}}$, $\overline{R_{bf}}$, $\overline{\delta_F}$, $\overline{\delta_{ff}}$, $\overline{\delta_{bf}}$, $\overline{\delta_{tr}}$, $\overline{\delta_{F\text{-}tr}}$, $\overline{m_{bf}}$ and $\overline{m_{tr}}$) are needed for the estimation of fuel $CO_2$ using the tracers CO and $\delta^{13}C(CO_2)$ (see Appendix A1 for derivation and Table 2 for summary of all equations). These parameters are dependent on the emission characteristics of the sources in the catchment area of the measurement site. If, for example, the mean isotopic signature of fuel $CO_2$ sources in the catchment area varies or if the catchment area itself varies, the integrated footprint-weighted parameter $\overline{\delta_F}$ will change. Typically, the integrated footprint-weighted parameters vary on timescales of hours, weeks, months and years. If, for a given measurement site, we could determine these parameters on the timescale of hours (which is the temporal resolution of our model), we would be able to estimate fuel $CO_2$ entirely correctly (difference of estimated and modeled fuel $CO_2$ would be zero) using CO and $\delta^{13}C(CO_2)$ or any combination of these tracers.

In contrast to methods using CO and/or $\delta^{13}C(CO_2)$, $CO_2$-only will overestimate fuel $CO_2$ when biospheric $CO_2$ contributions are positive (which will often be the case during nighttime and in winter) and underestimate fuel $CO_2$ when the biospheric $CO_2$ is negative (which may be the case during daytime in summer). This leads to time-dependent biases depending on the proportion of biospheric $CO_2$ to total $CO_2$ at the location, which is in general not negligible compared to the fuel $CO_2$ signal.

As $\Delta^{14}C(CO_2)$ is not sensitive to biofuel contributions, $\Delta^{14}C(CO_2)$-based fuel $CO_2$ estimates will underestimate the fuel $CO_2$ contributions approximately by the amount of biofuel $CO_2$ to the regional $CO_2$ concentration offset. Additionally, any $^{14}C(CO_2)$ emissions from nearby nuclear power plants or nuclear fuel reprocessing plants could potentially mask the depletion of fuel $CO_2$ contributions. Nuclear power plant emissions were not implemented in this model, but we will shortly discuss their possible effects in Sect. 5.

### 3.2 Low (monthly) resolution of parameters and variables

Normally it is not be possible to determine parameters such as $\overline{R_F}$, $\overline{R_{tr}}$, $\overline{R_{bf}}$, $\overline{\delta_F}$, $\overline{\delta_{ff}}$, $\overline{\delta_{bf}}$, $\overline{\delta_{tr}}$, $\overline{\delta_{F\text{-}tr}}$, $\overline{m_{bf}}$ and $\overline{m_{tr}}$ with hourly resolution. Thus we investigate how using monthly median values of these parameters may influence the fuel $CO_2$ estimates. We will discuss later how we can obtain their monthly mean values and for now we assume their monthly median value is known. Note that we use the median instead of the mean value for the footprint-weighted parameters, since the median is less sensitive to outliers. Using only monthly median values will introduce sub-monthly inaccuracies into the fuel $CO_2$ estimate since the footprint-weighted parameters vary on sub-monthly timescales. The variability in the discrepancy between estimated and reference (directly modeled) fuel $CO_2$ estimates will depend on the magnitude of sub-monthly variations of $\overline{R_F}$, $\overline{R_{tr}}$, $\overline{R_{bf}}$, $\overline{\delta_F}$, $\overline{\delta_{ff}}$, $\overline{\delta_{bf}}$, $\overline{\delta_{tr}}$, $\overline{\delta_{F\text{-}tr}}$, $\overline{m_{bf}}$ and $\overline{m_{tr}}$, as well as on their absolute values. For example, the more depleted the fuel $CO_2$ emissions are, the larger the isotopic difference between emissions from the biosphere and from fuel burning and the better the tracer $\delta^{13}C(CO_2)$ will be for fuel $CO_2$ emissions as both emission groups can be isotopically distinguished clearly (see Appendix C). For our model setting, the sub-monthly variations (standard deviation) are about $\pm 3$ $(\text{nmol mol}^{-1})/(\mu\text{mol mol}^{-1})$ for $\overline{R_F}$, $\overline{R_{tr}}$ and $\overline{R_{bf}}$; $\pm 0.2$ $(\text{nmol mol}^{-1})/(\text{nmol mol}^{-1})$ for $\overline{m_{bf}}$ and $\overline{m_{tr}}$; and $\pm 2$ ‰ for $\overline{\delta_F}$, $\overline{\delta_{ff}}$, $\overline{\delta_{bf}}$, $\overline{\delta_{tr}}$ and $\overline{\delta_{F\text{-}tr}}$ (variations due to varying footprints in the STILT model and temporal emission patterns of the different emission sectors). This variation is propagated into the fuel $CO_2$ estimate. The corresponding distribution of the difference between the estimated and modeled fuel $CO_2$ can be seen in Fig. 1 for the station Heidelberg and in Figs. 2 and 3 for Gartow and Berlin.

The mean difference between the modeled and tracer-based fuel $CO_2$ estimate provides a measure for the accuracy of the fuel $CO_2$ determination with the different tracer methods. In principle, one cannot assume that, when using the correct median values for $\overline{R_F}$, $\overline{R_{tr}}$, $\overline{R_{bf}}$, $\overline{\delta_F}$, $\overline{\delta_{ff}}$, $\overline{\delta_{bf}}$, $\overline{\delta_{tr}}$ and $\overline{\delta_{F\text{-}tr}}$, no median bias will be introduced into the $CO_2$ estimate. The reason is that the values for $\overline{R_F}$, $\overline{R_{tr}}$, $\overline{R_{bf}}$, $\overline{\delta_F}$, $\overline{\delta_{ff}}$, $\overline{\delta_{bf}}$, $\overline{\delta_{tr}}$ and $\overline{\delta_{F\text{-}tr}}$ are calculated on an hourly basis independent of the total fuel $CO_2$ value ($y_F$) at that time and are then averaged monthly. However, if $y_F$ and $\overline{R_F}$, $\overline{R_{tr}}$, $\overline{R_{bf}}$, $\overline{\delta_F}$, $\overline{\delta_{ff}}$, $\overline{\delta_{bf}}$, $\overline{\delta_{tr}}$ and $\overline{\delta_{F\text{-}tr}}$ are correlated, sub-monthly over- and underestimation of $y_F$ due to sub-monthly variation in $\overline{R_F}$, $\overline{R_{tr}}$, $\overline{R_{bf}}$, $\overline{\delta_F}$, $\overline{\delta_{ff}}$, $\overline{\delta_{bf}}$, $\overline{\delta_{tr}}$ and $\overline{\delta_{F\text{-}tr}}$ will not necessarily average out. An analysis of the bias (difference between modeled and tracer-based fuel $CO_2$ estimate; $x$ axis in Figs. 1–3) introduced when using monthly median footprint-weighted parameters is therefore vital. The standard deviations of the Gaussian fits to the difference distributions (Figs. 1–3) provide a measure for the precision of fuel $CO_2$ determination.

All methods using $\delta^{13}C(CO_2)$ and/or CO (Figs. 1b–e, 2b–e and 3b–e) are able to estimate fuel $CO_2$ without significant systematic biases if the annual median parameters $\overline{\delta_{ff}}$, $\overline{\delta_{bf}}$, $\overline{\delta_{tr}}$, $\overline{\delta_{F\text{-}tr}}$ and $\overline{R_F}$ are known (see Sect. 3.3. for the case that they are not accurately known). Mean and median differences of modeled and estimated fuel $CO_2$ are within 10 % of the annual mean fuel $CO_2$ signal. The benefit when using CO additionally to $\delta^{13}C(CO_2)$ is very small, which is due to the fact that traffic or biofuel $CO_2$ contributions are not very distinct with respect to their isotopic signature or their $CO\,/\,CO_2$ emission ratio from the other fuel $CO_2$ contributions for our model settings. When using CO as a tracer for fuel $CO_2$ (Figs. 1b, 2b and 3b) the standard deviation of the difference between the estimated and the true fuel $CO_2$ value is larger than when using $\delta^{13}C(CO_2)$. The reason is the large sub-monthly variation in footprint-weighted $\overline{R_F}$ in our modeled data.

Generally, the absolute standard deviation of the different tracer distributions is larger at the polluted station than at urban and rural stations. At the same time, we found that the variation in the footprint-weighted parameters such as $\overline{R_F}$, $\overline{R_{tr}}$, $\overline{R_{bf}}$, $\overline{\delta_F}$, $\overline{\delta_{ff}}$, $\overline{\delta_{bf}}$, $\overline{\delta_{tr}}$, $\overline{\delta_{F\text{-}tr}}$, $\overline{m_{bf}}$ and $\overline{m_{tr}}$ is largest in rural areas and smallest in polluted areas, which is probably due to the fact that the many polluters homogenize partly in polluted catchment areas, whereas the emissions of the few different polluters are temporally and spatially distinct at cleaner sites. Hence, the larger spread of the fuel $CO_2$ estimate at polluted stations is not the result of larger source heterogeneity but is rather due to the larger absolute signals (and with that larger absolute variations) of fuel $CO_2$ in the catchment area of these sites. Only $CO_2$ as a tracer for fuel $CO_2$ shows less variability at the polluted site Berlin, which is due to smaller contribution from the biosphere in its catchment area. However, the relative variability (i.e., $1\sigma\,/\,\text{mean}(y_F)$) is significantly higher in Gartow (e.g., the $\delta^{13}C$ method: 20 %) than it is in Heidelberg or Berlin (both ca. 5 %). Differences and spreads of the $CO_2$-only and $^{14}C(CO_2)$ method have already been described in Sect. 3.1.

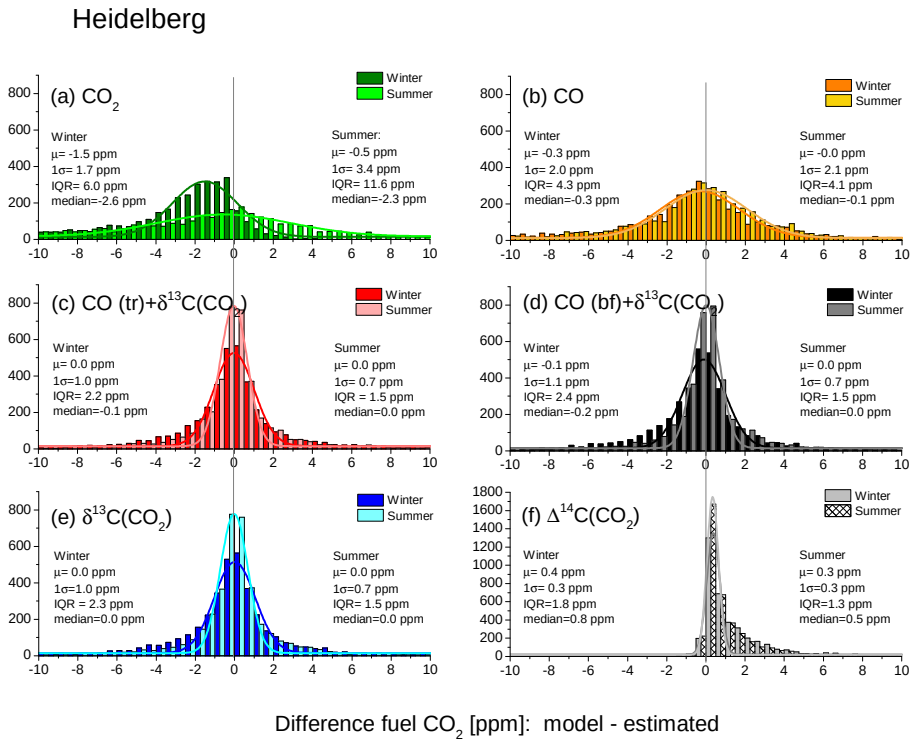


**Figure 1.** Histograms showing the differences between the modeled fuel $CO_2$ (assumed as correct) and the tracer-based estimated fuel $CO_2$ for the year 2012 for Heidelberg using the different tracers and tracer configurations listed in Table 2. Differences result from sub-monthly variations of parameters. Note the different $y$ axis scale. Darker colors denote the winter periods and lighter colors the summer periods (see legend). The distributions were fitted with a Gaussian fit and the shift ($\mu$) and the standard deviation ($\sigma$) for the Gaussian fits are given in the figure. Since the histograms do not follow Gaussian distributions (especially for $^{14}C(CO_2)$ due to non-normally distributed biofuel $CO_2$ contributions within 1 year) we also give the interquartile range (IQR) in the figure to remind the reader that the uncertainty may be underestimated when using the Gaussian standard deviation for uncertainty analysis. The $CO_2$ mole fractions are given in parts per million (ppm), which is equivalent to $\mu mol\,mol^{-1}$. Note that, in Heidelberg, mean fuel $CO_2$ for summer is 15 $\mu mol\,mol^{-1}$ and that for winter is 16 $\mu mol\,mol^{-1}$.

We have found that only small median differences occur when using $\delta^{13}C(CO_2)$ or CO as a tracer for fuel $CO_2$. This finding is only valid under the premise that the median values of all input and footprint-weighted parameters are known. If one or more of the parameters or variables are assigned incorrectly, this will lead to a systematic error of the fuel $CO_2$ estimate. The sensitivity of this misassignment for the different parameters and variables will be assessed in the next chapter.

### 3.3 Sensitivity of fuel $CO_2$ estimates on misassigned parameters and variables

We have investigated how well we are able to estimate fuel $CO_2$ in a setting in which, for example, the monthly averages of all parameters are perfectly well known but temporally varying on a shorter timescale. However, since, in reality, parameters such as $\overline{\delta_F}$ or $\overline{R_F}$ are only approximately known, we need to investigate how a misassignment of one of these parameters will influence fuel $CO_2$ estimates. This will provide information on how well certain parameters and variables need to be assigned for a fuel $CO_2$ estimate with targeted accuracy. For this purpose, we misassign one parameter and, at the same time, keep the other parameters at their correct value. We then determine how the fuel $CO_2$ estimate changes ($y$ axis in Fig. 4) when the misassignment of the parameter ($x$ axis) varies. The sensitivities of all methods to the most important parameters and variables are shown in Fig. 4 for example of the urban site Heidelberg. We have done this analysis for the parameters $CO_{2tot}$ (Fig. 4a), $\delta^{13}C_{tot}$ (Fig. 4b), $CO_{2bg}$ (Fig. 4c), $\delta^{13}C_{bg}$ (Fig. 4d), $\overline{\delta_F}$ (Fig. 4e), $\overline{\delta_{bio}}$ (Fig. 4f), $\overline{\delta_{bf}}$ (Fig. 4g), $\overline{\delta_{tr}}$ (Fig. 4h), CO offset (Fig. 4i), $\overline{m_{bf}}$ and $\overline{m_{tr}}$ (Fig. 4j), $\overline{R_{tr}}$ and $\overline{R_{bf}}$ (Fig. 4k), $\overline{R_F}$ (Fig. 4l), $\Delta^{14}C_{tot}$ (Fig. 4m), $\Delta^{14}C_{bg}$ (Fig. 4n), $\Delta^{14}C_{bio}$ (Fig. 4o), and $\Delta^{14}C_{bf}$ (Fig. 4p). The variation in these values was chosen in a way that the range includes the typical measurement precision for $CO_{2meas}$, $CO_{2bg}$, $\delta_{bg}$, $\delta_{meas}$, $\Delta^{14}C_{bg}$ and $\Delta^{14}C_{meas}$. The variation in the CO offset was chosen in a way that it displays the measurement precision of total CO and of the background CO but also includes realistic contributions from natural CO sources and sinks. For the parameters $\overline{R_F}$, $\overline{R_{tr}}$, $\overline{R_{bf}}$, $\overline{\delta_F}$, $\overline{\delta_{ff}}$, $\overline{\delta_{bf}}$,

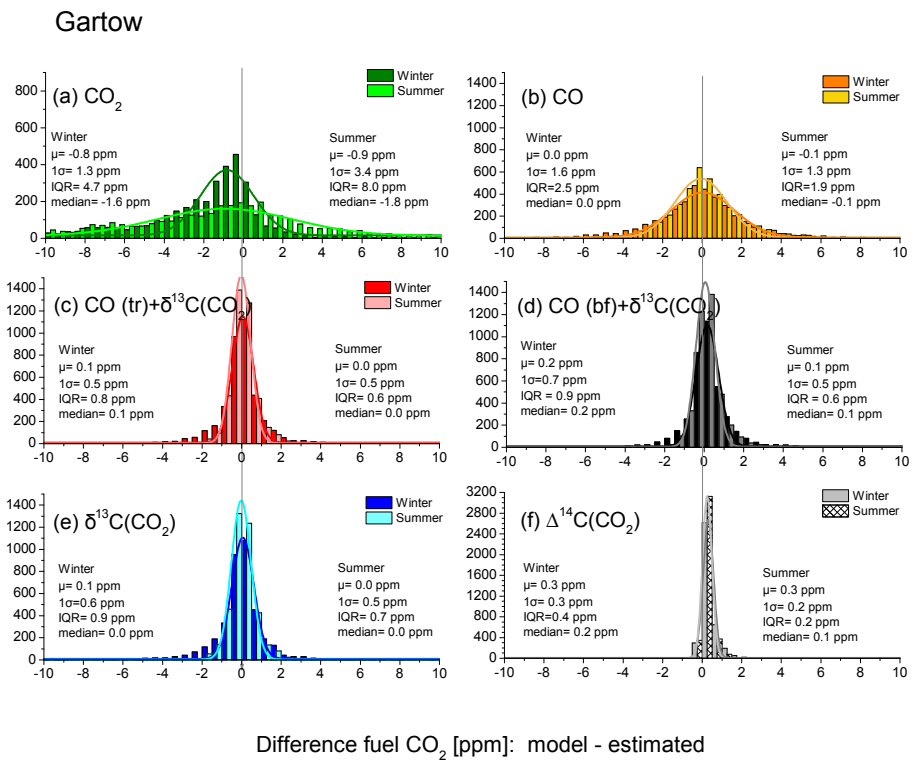


**Figure 2.** Same as Fig. 1 but for Gartow. In Gartow, mean fuel $CO_2$ for summer is 2 μmol mol$^{-1}$ and that for winter is 4 μmol mol$^{-1}$.

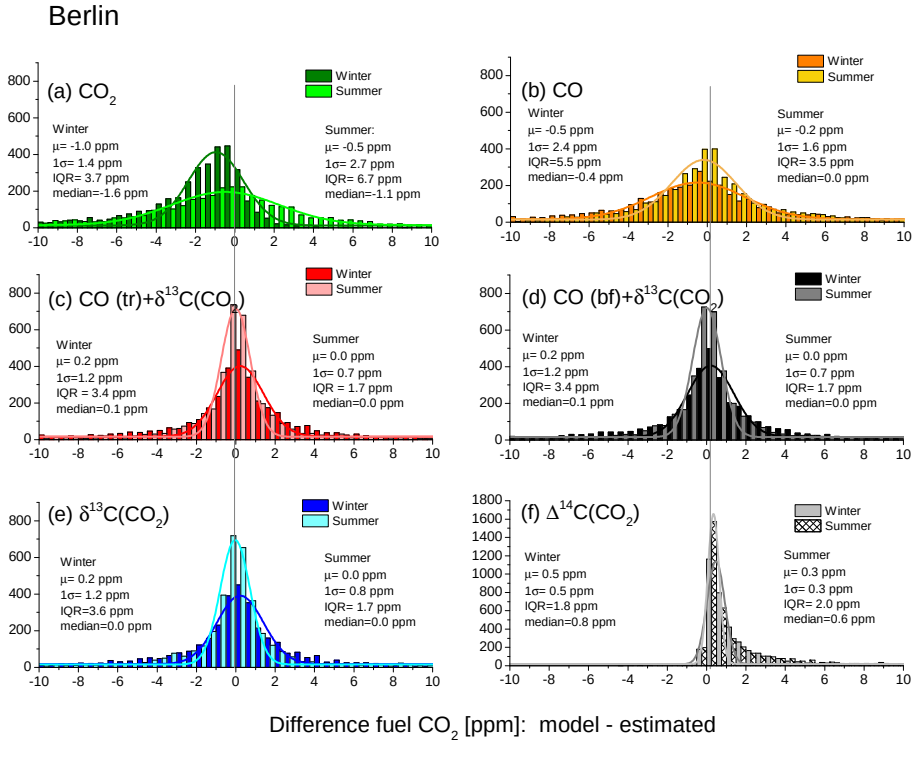


**Figure 3.** Same as Fig. 1 but for Berlin. In Berlin, mean fuel $CO_2$ for summer is 23 μmol mol$^{-1}$ and that for winter is 27 μmol mol$^{-1}$.

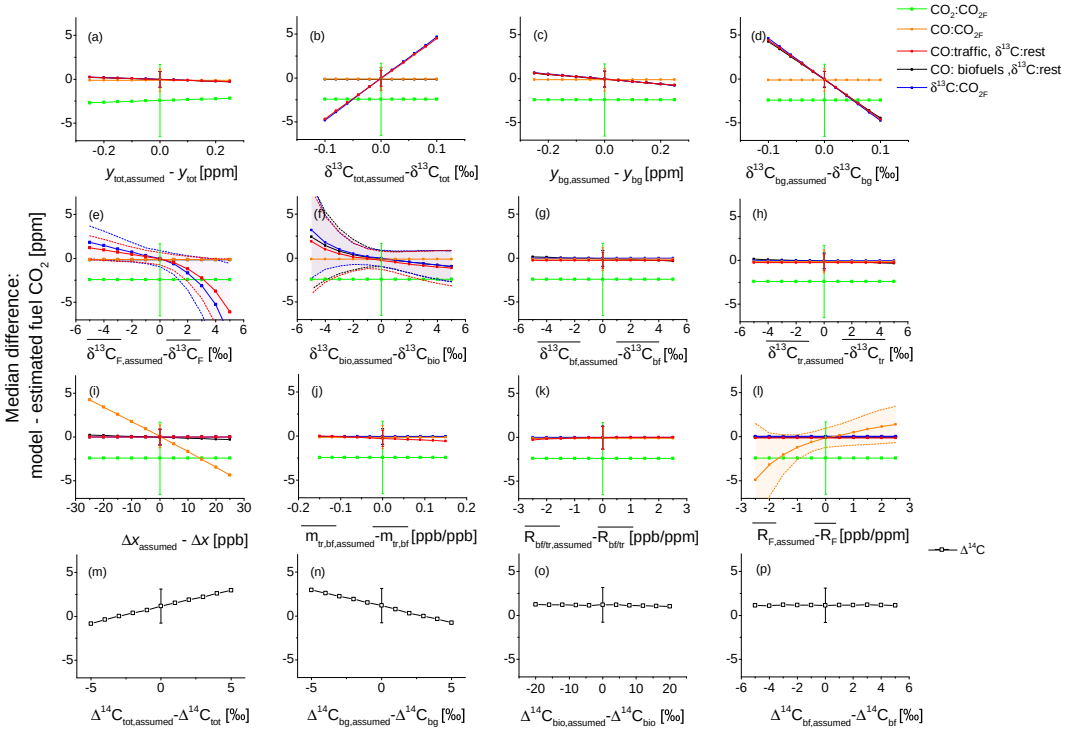


**Figure 4.** Sensitivity analysis: median difference between the modeled fuel $CO_2$ and the tracer-based estimated fuel $CO_2$ value ($y$ axis) at a typical urban site (Heidelberg) when using parameters/variables for fuel $CO_2$ estimation ("assumed") deviating from the correct parameters/variables used in STILT. The error bars given at $x = 0$ (assumed value = model value) denote the interquartile ranges (IQR) for all $x$ positions. If the IQRs vary depending on the assumed value, the errors (IQRs) are drawn as shaded areas.

$\overline{\delta_{tr}}$, $\overline{\delta_{F\text{-}tr}}$, $\overline{m_{bf}}$, and $\overline{m_{tr}}$ as well as for $\Delta^{14}C_{bio}$ and $\Delta^{14}C_{bf}$, we selected realistic ranges of sub-monthly parameter variation.

The error bars given at $x = 0$ of Fig. 4 show the interquartile ranges (IQR) and stem from the sub-monthly variability in $\overline{\delta_F}$, $\overline{R_F}$, $\overline{m_{bf}}$ and $\overline{m_{tr}}$, which was discussed in Sect. 3.2. One can directly identify critical parameters and variables for which the difference between the modeled and estimated fuel $CO_2$ ($y$ axis) changes significantly with increasing misassignment of parameters/variables ($x$ axis).

### 3.3.1 Sensitivity of $CO_2$-only method

We confirm that the $CO_2$-only method (green in Fig. 4) is insensitive to the variation in the displayed parameters/variables.

### 3.3.2 Sensitivity of CO method

Critical parameters/variables of the CO method (orange in Fig. 4) are the CO offset $\Delta$CO (Fig. 4i), as well as the ratio $\overline{R_F}$ ($= \Delta x / y_F$) (Fig. 4l). In practice, the CO offset is derived by subtracting the CO background as well as natural CO source and sink contributions from the total measured CO mole fraction. Typical fuel CO offsets are on the order of 40 nmol mol$^{-1}$. In our model we have not included natural CO sources and sinks, but in practice the uncertainty of the CO mole fraction measurement and of the natural CO contributions will add to the uncertainty of the fuel $CO_2$ estimate. Assuming, for example, a CO background which is 15 nmol mol$^{-1}$ too large, or assuming an additional sink resulting in a 15 nmol mol$^{-1}$ lower CO background, which may be a realistic diurnal variation in natural CO variation (Gros et al., 2002; Vogel, 2010), would lead to a significant overestimation of fuel $CO_2$ of about 2.5 µmol mol$^{-1}$ (median). Therefore, for a real data set, it is vital to determine the natural CO contributions and sinks (also soil sinks) using chemistry models or calibration with, for example, $\Delta^{14}C(CO_2)$ (see Sect. 4). In Heidelberg, the median modeled ratio $\overline{R_F}$ is about 5 (µmol mol$^{-1}$)/(nmol mol$^{-1}$) and shows a rather large variation of 3 (nmol mol$^{-1}$)/(µmol mol$^{-1}$). Figure 4l shows that such a variation in $\overline{R_F}$ contributes significantly to the imprecision of fuel $CO_2$ in the CO method. Also, the correct determination of $\overline{R_F}$ is vital for accurate fuel $CO_2$ estimates using CO.

### 3.3.3 Sensitivity of methods using $\delta^{13}C(CO_2)$

The sensitivities of fuel $CO_2$ estimates using $\delta^{13}C(CO_2)$ only (blue in Fig. 4) and combinations of $\delta^{13}C(CO_2)$ and CO are rather similar (red and black in Fig. 4). Note that the sensitivity on $\delta_{bg}$ or $\delta_{tot}$ is plotted when keeping $y_{bg}$ and $y_{tot}$ constant. Changing the $y_{bg}$ or $y_{tot}$ values at the same time

when changing $\delta_{bg}$ or $\delta_{tot}$ (following a Keeling curve (Keeling, 1958, 1960) with typical mean $\delta^{13}C$ source of $-25$ ‰) results in sensitivity about a factor of 10 smaller and is therefore not critical. However, small $\delta^{13}C(CO_2)$ variations (e.g., due to finite measurement precision or small inaccuracies) which are uncorrelated with $CO_{2tot}$ lead to large biases in fuel $CO_2$, e.g., a measurement bias of $\delta_{tot} = 0.1$ ‰, leads to a fuel $CO_2$ misassignment of 5 ($\mu mol\,mol^{-1}$) (see Fig. 4b). Therefore, a high measurement precision as well as accuracy of $\delta^{13}C(CO_2)$ is required for precise and accurate fuel $CO_2$ estimation. Further critical parameters of the methods using $\delta^{13}C(CO_2)$ are the isotopic signature of fuel $CO_2$ and the isotopic signature of biospheric $CO_2$ in the footprint (see Fig. 4e, f). The isotopic signatures of fuel and biospheric $CO_2$ must therefore be well known (or potentially calibrated; see Sect. 4) if we want to use $\delta^{13}C(CO_2)$ as a tracer for fuel $CO_2$. In particular, assuming more enriched fuel isotopic signatures or too depleted biospheric signatures biases the fuel $CO_2$ estimates strongly, because in these cases, biospheric and fuel $CO_2$ sources are difficult to distinguish using $\delta^{13}C(CO_2)$.

#### 3.3.4 Sensitivity of $\Delta^{14}C(CO_2)$ method

Figure 4m–p display the sensitivity of the $\Delta^{14}C(CO_2)$-based estimate of fuel $CO_2$ on the variables $\Delta^{14}C_{tot}$, $\Delta^{14}C_{bg}$ and $\Delta^{14}C_{bio}$. While fuel $CO_2$ is rather insensitive to misassignment of $\Delta^{14}C(CO_2)_{bio}$ (Fig. 4o) and $\Delta^{14}C(CO_2)_{bf}$ (Fig. 4p), it is very sensitive to $\Delta^{14}C(CO_2)_{tot}$ (Fig. 4m) and $\Delta^{14}C(CO_2)_{bg}$ (Fig. 4n) as has already been described in Turnbull et al. (2007). Thus, precise and accurate $\Delta^{14}C(CO_2)$ measurements are important for fuel $CO_2$ determination. Note that the best currently achieved measurement precision of conventional counting or AMS measurements is ±2 ‰ (equivalent to about $\pm 1.0\,\mu mol\,mol^{-1}$ fuel $CO_2$), but the hypothetical future continuous GC-AMS measurements may be on the order of ±5 ‰ (equivalent to about $\pm 3\,\mu mol\,mol^{-1}$ fuel $CO_2$). The reason why the fuel (biofuel + fossil fuel) $CO_2$ estimate based on $^{14}C$ is biased by about $1.1\,\mu mol\,mol^{-1}$ is due to the fact that biofuel $CO_2$, in contrast to fossil fuel $CO_2$, contains $^{14}C(CO_2)$ and is therefore not detectable through a lack of $^{14}C(CO_2)$.

### 3.4 Measurement precision and sub-monthly variation in parameters/variables

In Sects. 3.3.1–3.3.4, we have seen how sensitive the fuel $CO_2$ estimates are to the total mole fractions and $\delta/\Delta$ values. Since they have a large impact on the fuel $CO_2$ estimate, we now include their uncertainty in our analysis of precision of fuel $CO_2$ estimation. In order to display the effect of a limited measurement precision of $CO_2$, CO, $\delta^{13}C(CO_2)$ and $\Delta^{14}C(CO_2)$ we construct random realizations with mean value zero and a specific standard deviation. Additionally, we add a random variation to the CO offset and the biospheric/biofuel isotopic ($\delta/\Delta$) signature in order to simulate the effect of variability in CO to $CO_2$ ratio and of isotopic end members. These random uncertainties were not included in Sects. 3.1 and 3.2 and in Figs. 1–3. Note that in reality these variations may not be randomly distributed but have a distinct sub-monthly pattern. For example, we may introduce a systematic bias in one direction if we have unaccounted production of CO from VOCs or if we have unaccounted CO (e.g., soil) sinks. These sources and sinks will not occur randomly, but have a distinct sub-monthly pattern. Depending on the sign of the net natural CO flux, the bias may be positive or negative. However, for simplicity, we also include the natural CO variation here as a random vector as no natural CO sinks or sources are included in the modeled CO offset but we want to show the possible effect of their variation.

The random vectors which were used in this study in this study are summarized and explained in Table 3. The distributions of the difference between estimated (including measurement and parameter uncertainties and sub-monthly variations) and modeled fuel $CO_2$ can be seen in Figs. 5–7. Note that a possible misassignment of parameters or variables as investigated in Fig. 4 is not accounted for in either Figs. 1–3 or Figs. 5–7.

When including the measurement uncertainties and (input and footprint-weighted) parameter variability in the considerations, the mean bias remains unaltered, since the included uncertainty is random. However, the distributions of the CO and $\delta^{13}C(CO_2)$-based approaches for rural sites (such as Gartow), medium polluted sites (such as Heidelberg) and polluted sites (such as Berlin) widen significantly by about the same amount for all three sites. This is due to identical assumed measurement precisions and parameter variations. Since the absolute fuel $CO_2$ offset is larger in Berlin (annual modeled average ca. $25\,\mu mol\,mol^{-1}$) than in Heidelberg ($16\,\mu mol\,mol^{-1}$) and in Gartow ($3\,\mu mol\,mol^{-1}$), the relative variability ($=1\sigma/\,\mathrm{mean}(y_F)$) is smallest for the measurement site in Berlin (e.g., ca. 15 % for the $\delta^{13}C(CO_2)$ method) and largest for Gartow (110 % for the $\delta^{13}C(CO_2)$ method). At present, it is therefore questionable whether the estimation of continuous fuel $CO_2$ is possible at rural measurement sites. Even $\Delta^{14}C(CO_2)$ measurements with a precision of 5 ‰ result in a variability in fuel $CO_2$ of 60 %, but a $\Delta^{14}C(CO_2)$ precision of 2 ‰ would lead to a variability in fuel $CO_2$ of only 35 % at rural sites (not shown here). The reduced precision of fuel $CO_2$ estimates which we observe when including limited measurement precision into our considerations highlights again the necessity of performing precise atmospheric measurements of $\delta^{13}C(CO_2)$ and $CO_2$ if we want to use $\delta^{13}C(CO_2)$ as a tracer for fuel $CO_2$.

For urban sites, CO and $\delta^{13}C(CO_2)$-based methods show a very similar precision of about $4\,\mu mol\,mol^{-1}$ ($1\sigma$). At urban sites, $\delta^{13}C(CO_2)$ is slightly more precise than CO. It is worth pointing out that $CO_2$-only may be an adequate tracer for fuel $CO_2$ in polluted areas in the wintertime as absolute biases are small (< 4 %) and the precision (ca. 12 %) is rather good.

**Table 3.** Magnitude, physical reason and reference of parameter variation (included in Figs. 5–7).

| Component | Variation (random) | Physical reason for variation | Reference |
|---|---|---|---|
| $y_{tot}$, $y_{bg}$ | 0.05 µmol mol$^{-1}$ | measurement uncertainty | Hammer et al. (2013) |
| $\delta_{meas}$, $\delta_{bg}$ | 0.05 ‰ | measurement uncertainty | e.g., Tuzson et al. (2011); Vardag et al. (2015) |
| $x_{tot}$ | 15 nmol mol$^{-1}$ | natural CO sources and sinks | Gros et al. (2002); Vogel (2010) |
| $\delta_{bio}$ | 2 ‰ | heterogeneity of biosphere | compare with Pataki et al. (2003) |
| $\Delta^{14}C_{meas}$ , $\Delta^{14}C_{bg}$ | 5 ‰ | measurement uncertainty | McIntyre et al. (2013) |
| $\Delta^{14}C_{bio}$ | 5 ‰ | heterogeneity of biosphere and turnover times | compare with Taylor et al. (2015) |
| $\Delta^{14}C_{bf}$ | 10 ‰ | source/age of biofuels | – |
| $\overline{R_F}$, $\overline{R_{tr}}$, $\overline{R_{bf}}$, $\overline{\delta_F}$ $\overline{\delta_{ff}}$, $\overline{\delta_{bf}}$, $\overline{\delta_{tr}}$, $\overline{\delta_{F\text{-}tr}}$, $\overline{m_{bf}}$ and $\overline{m_{tr}}$ | – Sub-monthly variation already included as only monthly median values are used, but parameters vary at an hourly timescale | footprint or source mix change | |

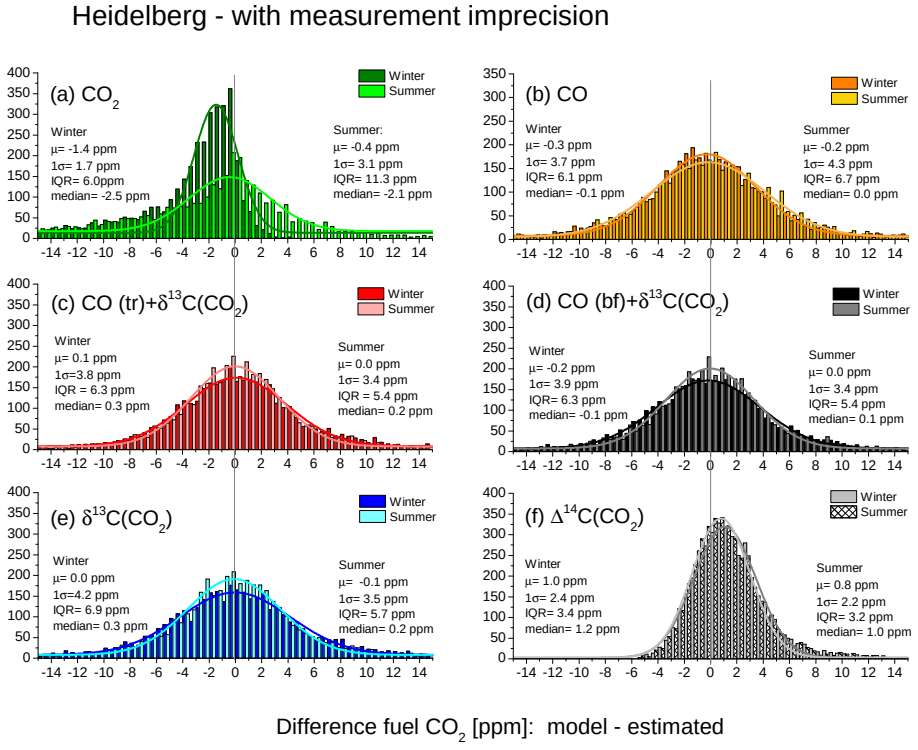


**Figure 5.** Same as Fig. 1 but now also including measurement imprecision.

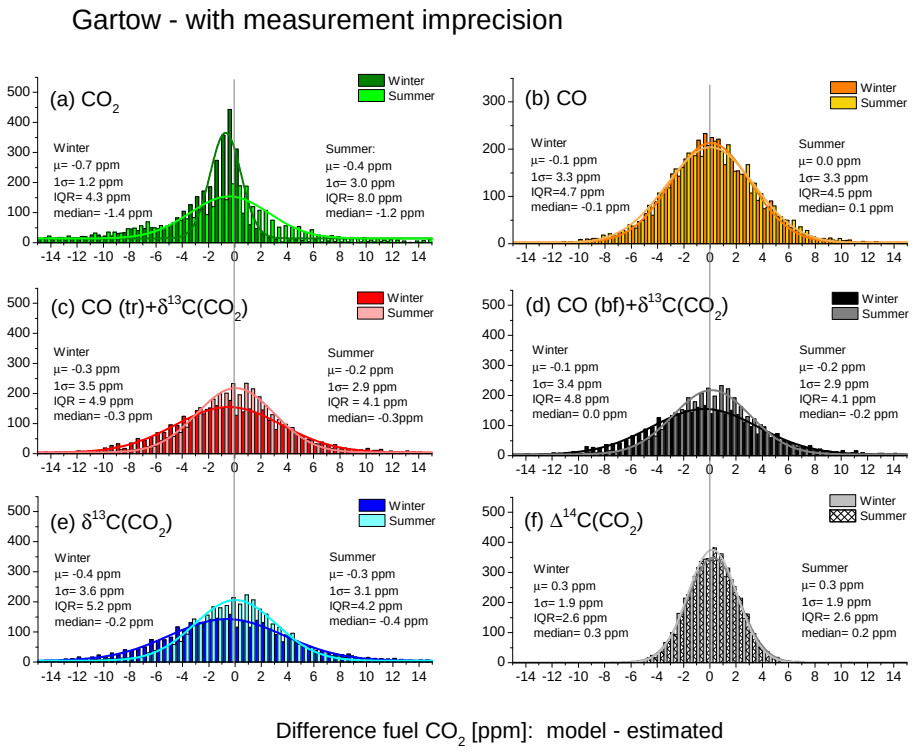


**Figure 6.** Same as Fig. 2 but now also including measurement imprecision.

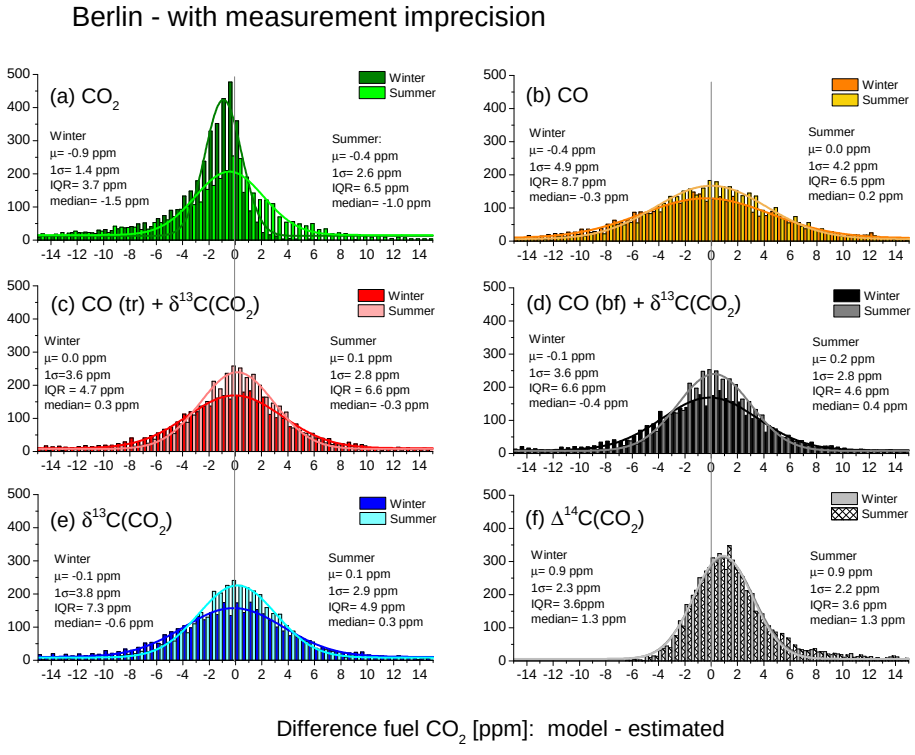


**Figure 7.** Same as Fig. 3 but now also including measurement imprecision.

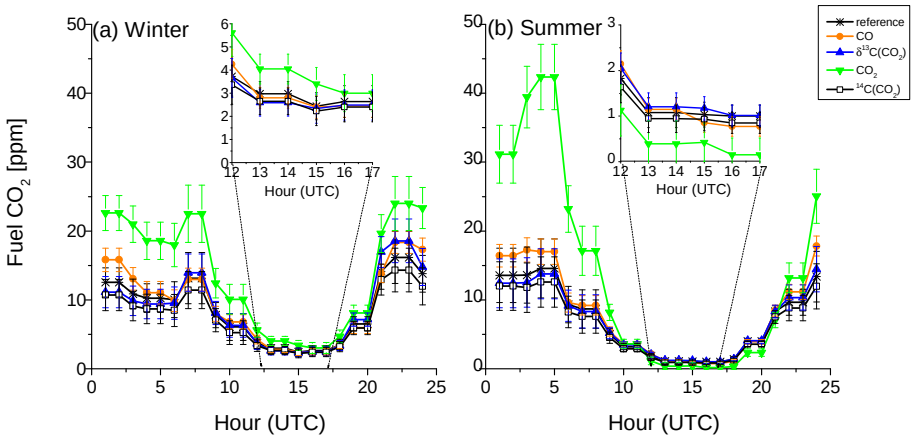


**Figure 8.** Comparison of median diurnal cycle of fuel $CO_2$ given in model reference or estimated with one of six different tracer methods at the measurement station Heidelberg. Error bars denote the standard error of the fuel $CO_2$ estimate at each hour for the respective half year. The diurnal cycle of the CO + $\delta^{13}C(CO_2)$ methods are not shown since they are very similar to the $\delta^{13}C(CO_2)$ method.

$\Delta^{14}C(CO_2)$ measurements with a precision of 5 ‰ would be the best tracer at all stations but are currently not available.

### 3.5 Comparison of the estimated fuel $CO_2$ diurnal cycle with different tracer configurations

As the diurnal cycle of $CO_2$ emissions is coupled to a diurnal change of the atmospheric mixing layer height, fuel $CO_2$ mole fraction varies during the day. In our calculations, we only use monthly median values of $\overline{R_F}$, $\overline{R_{tr}}$, $\overline{R_{bf}}$, $\overline{\delta_F}$, $\overline{\delta_{ff}}$, $\overline{\delta_{bf}}$, $\overline{\delta_{tr}}$, $\overline{\delta_{F\text{-}tr}}$, $\overline{m_{bf}}$ and $\overline{m_{tr}}$ for fuel $CO_2$ estimation. Discrepancies between the modeled reference diurnal cycle and the tracer-based diurnal cycle may be introduced due to a diurnal cycle of the parameters $\overline{R_F}$, $\overline{R_{tr}}$, $\overline{R_{bf}}$, $\overline{\delta_F}$, $\overline{\delta_{ff}}$, $\overline{\delta_{bf}}$, $\overline{\delta_{tr}}$, $\overline{\delta_{F\text{-}tr}}$, $\overline{m_{bf}}$ and $\overline{m_{tr}}$. We thus need to test whether we are able to reproduce the diurnal fuel $CO_2$ pattern in order to estimate fuel $CO_2$ from tracers at sub-diurnal resolution. Therefore, we calculate the median diurnal fuel $CO_2$ cycles with the different methods and compare them to the reference model diurnal cycle for summer and for winter (see Fig. 8 for the urban station Heidelberg).

One can see that the $\delta^{13}C(CO_2)$ method reproduces the reference diurnal cycle within its variability very well (standard errors of the respective hour in a half year are denoted as error bars in Fig. 8). Median hourly differences are about $0.1 \pm 0.7\,\mu mol\,mol^{-1}$ for methods using $\delta^{13}C(CO_2)$. The $CO_2$-only method largely overestimates fuel $CO_2$ contributions during the night by up to $10\,\mu mol\,mol^{-1}$ in winter and by about 15–25 $\mu mol\,mol^{-1}$ in summer. During the afternoon, the $CO_2$-only method overestimates fuel $CO_2$ in winter and underestimates it in summer. Even though the absolute difference is small during the afternoon, the relative difference is still large. The $CO_2$-only method is therefore not able to trace the diurnal fuel $CO_2$ variation at a site like Heidelberg correctly. Using $\Delta^{14}C(CO_2)$ for fuel $CO_2$ estimation leads to a slight median underestimation throughout the day (and season), which is due to the presence of $^{14}C(CO_2)$ in biofuel $CO_2$ masking all biofuel $CO_2$ contributions. The CO method slightly overestimates fuel $CO_2$ during nighttime by about 10 % in winter and 20 % in summer. The standard deviation of the hourly medians of the differences between model and CO-based fuel $CO_2$ is about 15 % of the total fuel $CO_2$.

One could consider implementing a diurnal correction into the fuel $CO_2$ estimate in a way that, in addition to monthly varying values for $\overline{R_F}$, $\overline{R_{tr}}$, $\overline{R_{bf}}$, $\overline{\delta_F}$, $\overline{\delta_{ff}}$, $\overline{\delta_{bf}}$, $\overline{\delta_{tr}}$, $\overline{\delta_{F\text{-}tr}}$, $\overline{m_{bf}}$ and $\overline{m_{tr}}$, hourly correction factors are implemented (see Vogel et al., 2010). This will be advantageous if the parameters exhibit a significant diurnal cycle themselves. However, for our setting, implementing a diurnal correction factor only slightly improves the agreement between the model and the estimated fuel $CO_2$ (not shown here). The reason is that the (hourly) median footprint-weighted parameters do not influence the (hourly) median fuel $CO_2$ estimates linearly, and that the synoptic variations of the footprint-weighted parameters are larger than the diurnal variations. Therefore, an hourly median correction factor does not necessarily improve the hourly fuel $CO_2$ estimate. We note that no diurnal systematic variability in the isotopic biospheric (respiration and photosynthesis) signature or in the non-fuel CO sinks and sources (which would be treated as an enhancement or reduction of the CO offset $\Delta$CO) was implemented but rather only random uncertainties of ±2 ‰ for $\delta_{bio}$ and $\pm 15\,nmol\,mol^{-1}$ for $\Delta$CO. This assumption of random variability will not be correct if systematic (e.g., diurnal) variation in $\delta^{13}C_{bio}$ and non-fossil $\Delta$CO variation occur. For $\delta^{13}C_{bio}$ the diurnal changes are expected to be small (< 1 ‰ (Flanagan et al., 2005) corresponding to fuel $CO_2$ biases of $< 0.5\,\mu mol\,mol^{-1}$), but for CO these may be larger (e.g., diurnal natural $\Delta$CO variation of about $10\,nmol\,mol^{-1}$ may occur from dry deposition of CO in forest soils during night and from photochemical production of CO by hydro-

carbons during the day (Gros et al., 2002) corresponding to ca. 2.5 µmol mol$^{-1}$ fuel $CO_2$). Therefore, in a real setting, it might be necessary to model natural CO concentration in order to not introduce a bias into diurnal $y_F$ structures.

In inverse model studies, often only afternoon hours are used to derive fluxes, as the atmospheric mixing can be better simulated by the models during conditions with a well-developed mixed layer (Gerbig et al., 2008). Therefore, it is especially important to check the afternoon values of fuel $CO_2$. Figure 8 shows an enlarged inlay of the diurnal cycle during the afternoon hours. Since in this model study we use the minimum of total $CH_4$ values within 2 days as a background value (Appendix A2), the afternoon offsets are very small, leading to a low signal-to-noise ratio. However, differences between the $\delta^{13}C(CO_2)$, CO, and $\Delta^{14}C(CO_2)$-based and reference fuel $CO_2$ are very small as well (mean differences < 10 % of afternoon fuel $CO_2$ value, standard deviation of differences about 30 %). Therefore, it seems justified to use an ensemble of afternoon values of continuous fuel $CO_2$ estimates (based on $\delta^{13}C(CO_2)$ or CO) for inverse model studies despite the small absolute fuel $CO_2$ values of about 1–2 µmol mol$^{-1}$ in the afternoon hours at an urban site.

## 4 Calibration of $\overline{\delta_F}$, $\overline{\delta_{F\text{-}tr}}$, $\overline{\delta_{ff}}$ and $\overline{R_F}$ with $\Delta^{14}C(CO_2)$ measurements

In order to estimate fuel $CO_2$ accurately with methods using CO and/or $\delta^{13}C(CO_2)$, the parameters $\overline{\delta_F}$, $\overline{\delta_{F\text{-}tr}}$, $\overline{\delta_{ff}}$ (and $\delta_{bio}$) and $\overline{R_F}$ need to be known with high accuracy, since biases are otherwise introduced into the fuel $CO_2$ estimate (see Fig. 4). However, for the evaluation of a measured data set, $\overline{\delta_F}$, $\overline{\delta_{F\text{-}tr}}$, $\overline{\delta_{ff}}$, $\delta_{bio}$ and $\overline{R_F}$ are not per se available but require either extensive source sampling campaigns or good bottom-up inventories. Alternatively, these parameters could also be "calibrated" using fossil fuel $CO_2$ estimates from $\Delta^{14}C(CO_2)$ measurements with high precision (in addition to biofuel contributions, which need to be added on top). For this purpose, Eqs. (1) and (2) can be rearranged and solved for calibration of $\overline{\delta_F}$, $\overline{\delta_{F\text{-}tr}}$, $\overline{\delta_{ff}}$ or $\overline{R_F}$ (for derivation see Appendix B).

Since $\Delta^{14}C(CO_2)$ measurements are time-consuming and costly, in practice only a limited number of $\Delta^{14}C(CO_2)$ measurements can be regularly performed. For example, in the Integrated Carbon Observation System (ICOS) atmospheric network, the radiocarbon measurement capacity was designed for about 50 radiocarbon measurements per station per year, of which about 26 will be used for integrated sampling for long-term monitoring of fossil fuel $CO_2$.

Previous radiocarbon calibration approaches have suggested integrated (e.g., monthly) sampling of $\Delta^{14}C(CO_2)$ for CO tracer calibration (cf. Levin and Karstens, 2007, and Vogel et al., 2010, for $\overline{R_F}$). Another possible approach for tracer calibration is to take grab samples rather than integrated samples (e.g., Turnbull et al., 2011). Grab samples could be taken throughout the year and the derived parameters $\overline{\delta_F}$, $\overline{\delta_{F\text{-}tr}}$, $\overline{\delta_{ff}}$, and $\overline{R_F}$ could then be averaged to one median value or separated into seasons and averaged to separate values, for instance, for summer and winter. The optimal sampling strategy depends on the structure, variation and noise of $\overline{\delta_F}$, $\overline{\delta_{F\text{-}tr}}$, $\overline{\delta_{ff}}$, and $\overline{R_F}$ within 1 year. Principally, it would also be possible to take all the samples consecutively at 2 h intervals during a so-called "event" and calculate the median value from the event. Therefore, we compare here four different sampling strategies for parameter calibration, all using a total of $n$ samples per year (in ICOS: $n \approx 24$). Note that we include sub-monthly variation in the parameters and measurement uncertainties in the observations (as in Sect. 3.4).

1. Integrated sample calibration: take $n/24$ integrated samples each month and their associated background samples (for $n \approx 24$, consisting of 12 monthly integrated samples at the measurement station as well as 12 monthly integrated samples at the background station) and calibrate $\overline{\delta_F}$, $\overline{\delta_{F\text{-}tr}}$, $\overline{\delta_{ff}}$, and $\overline{R_F}$ on a monthly basis from the integrated samples (this corresponds to the approach suggested by Levin and Karstens, 2007, and Vogel et al., 2010, for $\overline{R_F}$). In this approach, the mean $\Delta CO$ and fuel $\Delta CO_2$ (from integrated CO and $\Delta^{14}C(CO_2)$ sampling) over the course of 1 month are used to calculate monthly $\frac{\Delta x}{\Delta y_F}$. However, since the mean of ratio $< \overline{R_F} > = < \frac{\Delta x}{\Delta y_F} >$ is actually required, and not the ratio of means $\frac{<\Delta x>}{<\Delta y_F>}$ (Vogel et al., 2010), biases may be introduced into the fuel $CO_2$ estimate (the same holds for the factors in $\overline{\delta_F}$, $\overline{\delta_{F\text{-}tr}}$ and $\overline{\delta_{ff}}$).

2. Annual grab sample calibration: randomly select a number of samples $n/2$ (and their associated afternoon background $(n/2)$) each year and calibrate annual median $\overline{\delta_F}$, $\overline{\delta_{F\text{-}tr}}$, $\overline{\delta_{ff}}$, and $\overline{R_F}$. Biases introduced by this sampling strategy are twofold. First, the random choice of grab samples may not represent the median annual value. This potential bias decreases with increasing number of grab samples used. Second, the potential seasonal cycle of the parameters is not considered. Therefore, in the annual grab sample calibration, the wintertime and summertime fuel $CO_2$ estimates will always be shifted against each other if $\overline{\delta_F}$, $\overline{\delta_{F\text{-}tr}}$, $\overline{\delta_{ff}}$, and $\overline{R_F}$ exhibit a seasonal cycle, but only one annual median value for these parameters would be used.

3. Seasonal grab sample calibration: randomly select a number of samples $n/4$ (and their associated afternoon background $(n/4)$) in summer and in winter and calibrate a median $\overline{\delta_F}$, $\overline{\delta_{F\text{-}tr}}$, $\overline{\delta_{ff}}$, and $\overline{R_F}$ with half-yearly resolution. Here, again, the random choice of grab samples may not represent the median half annual value, and a potential bias may be even larger here than in the annual grab sample calibration, since only half the samples are available to obtain a robust value for $\overline{\delta_F}$, $\overline{\delta_{F\text{-}tr}}$, $\overline{\delta_{ff}}$, and

**Table 4.** Absolute mean difference of tracer-based estimate and modeled (assumed as correct) fuel $CO_2$ in µmol mol$^{-1}$ for the tracers CO and $\delta^{13}C(CO_2)$ for different sampling strategies and respective standard deviation (both determined from a Gaussian fit to the difference histogram) for an urban setting (here: Heidelberg). Depending on the random selection of grab samples, the bias of the calibration with annually distributed grab samples is sometimes positive and sometimes negative. Therefore, the mean absolute difference between the modeled and calibrated value was determined in a Monte Carlo simulation and is shown with a "±" sign in front of the mean value to show that the bias does not have a unique sign. The standard deviation denotes the $1\sigma$ uncertainty of the difference, which is always bidirectional. Note that we only show the results for CO and $\delta^{13}C(CO_2)$, since the results when using a combination of these tracers are very similar to those of the $\delta^{13}C(CO_2)$ method. Measurement uncertainties are included in all calibration methods.

| Method | | CO mole fraction | | $\delta^{13}C$-$CO_2$ | |
|---|---|---|---|---|---|
| | | Summer | Winter | Summer | Winter |
| No uncertainties, monthly median values known (as shown in Fig. 1) | | $0.0 \pm 2.1$ | $-0.3 \pm 2.0$ | $0.0 \pm 0.7$ | $0.1 \pm 1.0$ |
| Measurement uncertainties included, monthly median values known (as shown in Fig. 5) | | $-0.2 \pm 4.3$ | $-0.3 \pm 3.7$ | $-0.1 \pm 3.5$ | $0.0 \pm 4.2$ |
| Calibration with integrated samples (method 1) | $n$=24 | $-0.8 \pm 4.9$ | $-0.7 \pm 4.0$ | $-2.4 \pm 5.2$ | $-1.8 \pm 5.1$ |
| Calibration with annually distributed grab samples (method 2) | $n$=24 | $\pm 1.2 \pm 5.3$ | $\pm 1.5 \pm 4.7$ | $\pm 0.8 \pm 4.0$ | $\pm 1.6 \pm 4.9$ |
| | $n$=96 | $\pm 1.1 \pm 5.2$ | $\pm 1.3 \pm 4.5$ | $\pm 0.5 \pm 3.8$ | $\pm 1.1 \pm 4.5$ |
| Calibration with seasonal grab sample calibration (method 3) | $n$=24 | $\pm 1.2 \pm 5.3$ | $\pm 1.5 \pm 4.7$ | $\pm 1.6 \pm 4.6$ | $\pm 1.6 \pm 4.9$ |
| | $n$=96 | $\pm 0.8 \pm 4.8$ | $\pm 1.1 \pm 4.3$ | $\pm 0.9 \pm 4.3$ | $\pm 0.8 \pm 4.3$ |
| Seasonal event calibration (method 4) | $n$=24 | $\pm 2.1 \pm 6.1$ | $\pm 2.0 \pm 5.1$ | $\pm 1.2 \pm 4.3$ | $\pm 1.9 \pm 5.1$ |
| | $n$=96 | $\pm 1.5 \pm 5.6$ | $\pm 1.9 \pm 4.9$ | $\pm 1.1 \pm 4.2$ | $\pm 1.3 \pm 4.6$ |

$\overline{R_F}$ for summer and winter. In return, it is in principal possible to detect the seasonal variation in $\overline{R_F}$ and $\overline{\delta_F}$, $\overline{\delta_{F\text{-tr}}}$, $\overline{\delta_{ff}}$.

4. Seasonal event calibration: Randomly select an "event day" each season. On this day, select $n/2-2$ consecutive grab samples (and one associated afternoon background) and calibrate a median $\overline{R_F}$ and $\overline{\delta_F}$, $\overline{\delta_{F\text{-tr}}}$, $\overline{\delta_{ff}}$ with half-yearly resolution. This approach is similar to approach 3 but entails a greater risk of choosing an event, which is not representative of the entire season, since subsequent samples are not independent of each other. On the other hand, it has the advantage of using more calibrations for the same number of radiocarbon measurements than approach 3 since only one background sample is needed for each event. However, if the background sample is biased, it will influence the entire event.

Comparing these sampling strategies to each other using one model run is difficult, since the result changes from random realization to random realization, depending on the selection of calibration samples in sampling strategy 2–4. We have therefore performed a Monte Carlo simulation (with 500 runs) and used the root median square difference between the obtained and originally modeled reference values $\overline{R_F}$ and $\overline{\delta_F}$, $\overline{\delta_{F\text{-tr}}}$, $\overline{\delta_{ff}}$ to calculate the difference between tracer-based estimate and modeled reference fuel $CO_2$.

Table 4 shows the absolute mean difference and standard deviation (as determined from a Gaussian fit to the difference histogram of modeled and tracer-based fuel $CO_2$, in analogy to Fig. 5) for an urban setting. One can see that the "integrated sample calibration" causes biases due to the covariance of the factors in Eqs. (B1)–(B4). The effect is much stronger for methods using $\delta^{13}C$ (ca. 15 % of mean fuel $CO_2$ offset in Heidelberg (16 µmol mol$^{-1}$)) than it is for the CO method (ca. 5 %). This bias is directed meaning that it is not a random uncertainty but actually a systematic bias introduced by computation. This is different from the calibrations on grab samples, which have a bidirectional absolute difference. Bidirectional differences may be advantageous over unidirectional differences when analyzing long-term records as bidirectional differences contribute to long-term noise rather than biases. For CO, it seems that the integrated calibration approach works well, but a uni-directed bias remains. Note that the differences found here are not due to the insensitivity of biofuel $CO_2$ contributions of $\Delta^{14}C(CO_2)$, as we add the (assumed as known) biofuel $CO_2$ prior to "calibration" (see Eqs. B1–B3).

We further find that, since $\overline{\delta_F}$, $\overline{\delta_{F\text{-tr}}}$ $\overline{\delta_{ff}}$, and $\overline{R_F}$ do not exhibit a strong annual cycle but show rather large, high-frequent variations, the best sampling strategy for 24 available radiocarbon measurements per year (as would be the case for the ICOS network) is using all available samples to calibrate well-defined median annual values of $\overline{\delta_F}$, $\overline{\delta_{F\text{-tr}}}$

$\overline{\delta_{\mathrm{ff}}}$, and $\overline{R_{\mathrm{F}}}$ (sampling strategy 2). With 96 (or more) available radiocarbon measurements, it may only be advisable to group the calibrations into half-yearly intervals. Having such many radiocarbon grab samples available may be a realistic scenario if the parameters do not show any trend over the course of several years. Note that a monthly grab sample calibration (not shown here) results in large biases of about $\pm 3\,\mu\mathrm{mol\,mol}^{-1}$ for CO-based as well as $\delta^{13}\mathrm{C}(\mathrm{CO_2})$-based methods and is thus not advisable.

The accuracy of the seasonal event calibration is slightly worse than the accuracy of the seasonal calibration (see Table 4) due to non-representativeness of a single event for the entire season.

## 5 Discussion and conclusion

In this work, we analyzed the advantages and disadvantages of different tracers for estimating continuous fuel $CO_2$ at different types of measurement stations. The accuracy and precision of continuous fuel $CO_2$ estimates at three example stations – one rural, one urban and one polluted site – were calculated. This should serve as orientation for the development of an atmospheric measurement strategy, so that the best tracer configuration for a particular station can be chosen to resolve the different $CO_2$ source components over a country or region. The results can be used to plan and construct new measurement networks and sampling strategies with the goal of deriving fuel $CO_2$ concentrations at high temporal resolution.

The results of our model study suggest that, with our current measurement precision of continuous tracers such as CO or $\delta^{13}\mathrm{C}(\mathrm{CO_2})$ (or $\Delta^{14}\mathrm{C}(\mathrm{CO_2})$), in general it is not possible to estimate fuel $CO_2$ in rural areas ($5\,\mu\mathrm{mol\,mol}^{-1}$ or less of fuel $CO_2$) with a precision better than 100 % (due to the small signal-to-noise ratio). It could still be possible to monitor single pollution events since the signal-to-noise ratio is much higher during such events. At present, it does not thus seem helpful to equip measurement stations in rural areas with continuous $\delta^{13}\mathrm{C}(\mathrm{CO_2})$ and CO measurements with the objective of monitoring continuous fuel $CO_2$. However, it seems that tracer-based fuel $CO_2$ monitoring may be possible at urban or polluted sites (as planned, for example, within the Megacities Carbon Project) and may have the potential to improve the fuel $CO_2$ bottom-up inventories.

We find that $CO_2$-only cannot be used as a tracer for fuel $CO_2$, as a significant contribution of $CO_2$ is released or taken up by the biosphere even in wintertime. Only during winter in strongly polluted areas do biogenic $CO_2$ contributions lead to a relatively small bias of about 5 % with the $CO_2$-only approach and a small variation ($\sigma$ / mean($y_{\mathrm{F}}$): 5 %; see Fig. 7).

In contrast to $CO_2$-only, CO and $\delta^{13}\mathrm{C}(\mathrm{CO_2})$ can be used as a tracer for fuel $CO_2$ in summer and in winter at urban and polluted sites. The accuracy of CO- and/or $\delta^{13}\mathrm{C}(\mathrm{CO_2})$-based fuel $CO_2$ estimates depends to a large degree on how well the different parameters such as $\overline{R_{\mathrm{F}}}$, $\overline{\delta_{\mathrm{F}}}$, and $\delta_{\mathrm{bio}}$ are known. Misassignment leads to significant biases in the fuel $CO_2$ estimate (Fig. 4). Therefore, in practice, it is important to screen and monitor all sources and sinks in the catchment area of the measurement site and to determine the median isotopic source signature and the median ratios $\overline{R_{\mathrm{F}}}$, $\overline{R_{\mathrm{tr}}}$, $\overline{R_{\mathrm{bf}}}$ as well as the CO offset as accurately as possible, for example, by calibration with co-located $\Delta^{14}\mathrm{C}(\mathrm{CO_2})$ measurements. The accuracy of the fuel $CO_2$ estimate after $^{14}\mathrm{C}$ calibration depends strongly on the number of radiocarbon samples available for calibration and on the sampling strategy used. For example, in the ICOS project, approximately 24 radiocarbon samples will be available for calibration of $\overline{R_{\mathrm{F}}}$, $\overline{\delta_{\mathrm{F}}}$, $\overline{\delta_{\mathrm{ff}}}$, or $\overline{\delta_{\mathrm{F\text{-}tr}}}$. With that number of calibration samples available, due to the large noise of the calibrated footprint-weighted parameters $\overline{\delta_{\mathrm{F}}}$ $\overline{\delta_{\mathrm{ff}}}$, or $\overline{\delta_{\mathrm{F\text{-}tr}}}$, it may be advantageous to group all calibrations to obtain robust annual median values for $\overline{\delta_{\mathrm{F}}}$, $\overline{\delta_{\mathrm{ff}}}$, or $\overline{\delta_{\mathrm{F\text{-}tr}}}$. If a large number of precise radiocarbon measurements are available, or if the parameters do not change over the course of several years and thus several years of calibration samples can be accumulated, it is advantageous to apply radiocarbon calibrations at half-yearly resolution. Note that due to changes in technology and technical processes, as well as due to a year-to-year variation in extreme temperatures, the contribution from fuel $CO_2$ different sectors is likely to change within a period of four years. However, this could be checked, for example, using nighttime Keeling plot intercepts (Vardag et al., 2015). For calibration of $\overline{R_{\mathrm{F}}}$, integrated $\Delta^{14}\mathrm{C}(\mathrm{CO_2})$ calibration could be used with rather small but systematic biases or grab samples could be used for slightly larger but random uncertainty. The accuracy will then typically be better than 10 % for the CO method or the $\delta^{13}\mathrm{C}(\mathrm{CO_2})$ method.

The precision of CO- and $\delta^{13}\mathrm{C}(\mathrm{CO_2})$-based approaches is very similar for all site classes, but for polluted sites $\delta^{13}\mathrm{C}(\mathrm{CO_2})$ seems slightly more precise. For Heidelberg it is about 25 % (e.g., $1\sigma$ / mean($y_{\mathrm{F}}$)). For CO, the uncertainty originates mainly from the large variation in $\overline{R_{\mathrm{F}}}$ in our model runs due to the inhomogeneity of fuel CO sources in the footprint area of urban or polluted measurement stations and due to natural CO sources. The uncertainty of the $\delta^{13}\mathrm{C}(\mathrm{CO_2})$ approach is mainly determined by the limited measurement precision of $\delta^{13}\mathrm{C}(\mathrm{CO_2})$. Thus in order to use $\delta^{13}\mathrm{C}(\mathrm{CO_2})$ as a tracer for fuel $CO_2$ it is vital to perform isotopic measurements with a precision of at least 0.05 ‰. The combination of $\delta^{13}\mathrm{C}(\mathrm{CO_2})$ and CO for fuel $CO_2$ estimation is favorable in cases where each of two emission groups is well distinguishable by one of the tracers. Since for our model setting this is only partly the case (EDGAR emission inventory; see Table A1), the combination of these tracers provides only little additional information.

We have found that hypothetical future $\Delta^{14}\mathrm{C}(\mathrm{CO_2})$ measurements with 5 ‰ absolute precision of background and measured $\Delta^{14}\mathrm{C}(\mathrm{CO_2})$ values (see Figs. 5f–7f) would generally be a very precise tracer for continuous fuel $CO_2$ es-

timation at rural ($1\sigma$ / mean($y_F$) $\approx 60\,\%$), urban (ca. 15 %) and polluted (ca. 10 %) stations. The precision of fuel $CO_2$ estimates is determined mainly by the limited measurement precision of background and total $\Delta^{14}C(CO_2)$ ($\pm 5$ ‰). Note, however, that $\Delta^{14}C(CO_2)$ measurements with 5 ‰ precision are not yet fully developed and commercially available. For comparison, a $\Delta^{14}C(CO_2)$ measurement precision of 1 % would be needed to achieve a fuel $CO_2$ precision similar to that of $\delta^{13}C(CO_2)$- and CO-based methods. An uncertainty of 2 %, which could be a realistic near-future precision of laser-based instruments (Galli et al., 2013), would lead to relative uncertainties of 260, 50 and 30 %, respectively. The downside of $\Delta^{14}C(CO_2)$ is its inability to determine biofuel $CO_2$. Therefore, the $\Delta^{14}C(CO_2)$ methods will underestimate the fuel $CO_2$ (biofuel plus fossil fuel) contributions approximately by the share of biofuel in $CO_2$ at the site. This may be only a small contribution, as was the case for the studied year 2012 (e.g., 5 % in Heidelberg), but may increase in the future. Note also that we have not investigated the effect of nuclear power plant $^{14}C(CO_2)$ contributions at the measurement site, which could additionally bias fuel $CO_2$ estimates derived from $\Delta^{14}C(CO_2)$ measurements. Dispersion model results for Heidelberg (M. Kuderer, personal communication, 2015) suggest that the nuclear power facilities (most importantly Philippsburg, located about 25 km southwest of Heidelberg) increase monthly mean $\Delta^{14}C(CO_2)$ by about $(2 \pm 2)$ ‰, corresponding to a misassignment in fuel $CO_2$ of about $0.8 \pm 0.8\,\mu mol\,mol^{-1}$ ($\approx 5\,\%$). If there are nuclear power plants or fuel reprocessing plants in the catchment area of the measurement site and if monthly mean emission data of pure $^{14}C(CO_2)$ from these nuclear facilities are available, it is advisable to correct for them at the highest possible temporal resolution using, for example, transport models (Vogel et al., 2013b). Note that for the calibration of $\overline{R_F}$, $\overline{\delta_F}$, $\overline{\delta_{ff}}$ or $\overline{\delta_{F\text{-}tr}}$ using $\Delta^{14}C(CO_2)$ grab samples, it should be possible to choose the calibration grab samples via trajectory forecast such that no nuclear power plant influences are encountered in the grab samples. However, this limits the footprint area that can be sampled and calibrated.

We have compared the diurnal cycle of the tracer-based fuel $CO_2$ estimates for Heidelberg and found that the tracer configurations using CO, $\delta^{13}C(CO_2)$ and $\Delta^{14}C(CO_2)$ were able to reproduce the diurnal cycle well and show a mean difference of better than $5 \pm 15\,\%$ and a root mean square difference of 15 % at the most. This seems surprising, since one might expect a diurnal pattern of $\overline{\delta_F}$ and $\overline{R_F}$ due to a varying share of emissions of different emission sectors in the footprint, leading to a systematic deviation of the estimated from the real modeled diurnal cycle. However, since the diurnal patterns are small (e.g., peak-to-peak difference of $\delta^{13}C(CO_2)$ ca. 2 ‰), the mean diurnal variations are not significantly improved when using a diurnal correction of the mean isotopic source signatures. One should keep in mind that natural CO contributions may also vary systematically on a diurnal basis. Such a natural systematic variation was not included in the model simulation but will potentially introduce a diurnal bias into the continuous fuel $CO_2$ estimate in a real setting. Therefore, it may be necessary to model or approximate natural CO in a real setting. It may be possible to approximate the (sub-monthly) natural CO component using formaldehyde (HCHO) measurements, since the production of CO from NMHC passes HCHO as an intermediate molecule (Atkinson, 2000). However, the high dry deposition rate of HCHO may complicate the interpretation further. Since afternoon values are often used in inverse model studies to derive fluxes, it is important that afternoon fuel $CO_2$ values can be estimated accurately. This could be confirmed for $\delta^{13}C(CO_2)$ and CO in this study (see Fig. 8).

In order to better study the biospheric carbon fluxes on all relevant scales, it is important to improve fuel $CO_2$ bottom-up inventories, so that fuel and biospheric $CO_2$ can be separated for independent use in inverse model approaches. At present, emission inventories typically have uncertainties of 30–150 % at regional resolution (Wang et al., 2013). We were able to show in our study that some tracer-based approaches such as CO and $\delta^{13}C(CO_2)$-based methods lead to uncertainties of fuel $CO_2$ of 30 % and accuracies of 10 % (after calibration). However, for retrieving improved emission estimates using inverse models, also the model transport errors need to be taken into account and convoluted with the accuracy of fuel $CO_2$ estimates. At the moment, the model transport errors are usually larger during nighttime (ca. 100 %) than in the afternoon (ca. 40 %) (excluding at mountain sites), which is why mainly afternoon values are used in model inversions (Gerbig et al., 2008). Obviously, but unfortunately during the afternoon hours, the fuel $CO_2$ signal is very small, complicating the unbiased estimation of fuel $CO_2$ emissions using continuous tracers in inverse transport models in these hours until better transport models and boundary layer height models exist.

## Appendix A: Methods of continuous fuel $CO_2$ determination

### A1 Tracer configurations and their emission groups

We formally introduce six different tracers or tracer combinations, which we use to estimate fuel $CO_2$ continuously: $CO_2$ is used as the sole tracer for fuel $CO_2$. CO, $\delta^{13}C(CO_2)$ and $\Delta^{14}C(CO_2)$ records are each used solely with $CO_2$ to estimate fuel $CO_2$. Further, CO is used as a tracer for traffic (and $\delta^{13}C(CO_2)$ as a tracer for fuel $CO_2$ minus traffic) and finally CO is used as a tracer for biofuels (and $\delta^{13}C(CO_2)$ as a tracer for fuel $CO_2$ minus biofuels). The different emission groups are also listed and characterized in Table A1.

#### A1.1 $CO_2$ as the sole tracer for fuel $CO_2$

When using $CO_2$ alone as "tracer" for fuel $CO_2$ ($y_F = y_{ff} + y_{bf}$), the total regional $CO_2$ offset is assumed to solely origi-

**Table A1.** Annual or half-yearly (summer: S; winter: W) averaged $\Delta^{14}C(CO_2)$, $\delta^{13}C(CO_2)$, $\Delta CO / \Delta CO_2$ ratios, and mean fraction of $CO_2$ and CO relative to total $CO_2$ and CO offsets as used in our model study for the measurement site Heidelberg for the year 2012. Biosphere $\Delta^{14}C(CO_2)$ values are based on Taylor et al. (2015). The $\Delta CO / \Delta CO_2$ ratio and the fractions of $CO_2$ and CO offset were taken from the STILT model runs, which were fed with anthropogenic emissions from the EDGAR emission inventory. Note that fractions of biofuels in traffic $CO_2$ emissions are not included. $\delta$ values were derived by assigning an isotopic value to each fuel type and weighting these depending on the respective share of the fuel type to total fuel $CO_2$ at the measurement site. The $\delta$ values of the biosphere are the half-yearly mean values from Table 1. Analogously, $R_x$ (and $\Delta^{14}C_x$) values were derived by assigning an emission ratio $CO / CO_2$ (and $\Delta^{14}C(CO_2)$value) to each emission sector and weighting these depending on the respective share of the emission sector to total fuel $CO_2$ at the site.

| Emission group | $\Delta^{14}C$-$CO_2$[‰] | $\delta^{13}C$ [‰] | | $\overline{R}_x = (\Delta CO / \Delta CO_2)_x$ | % of $\Delta CO_2$ | | % of $\Delta CO$ | |
|---|---|---|---|---|---|---|---|---|
| | | S | W | [ppb ppm$^{-1}$] | S | W | S | W |
| Fuel $CO_2$ | −995 | −31.5 | −33.5 | 7 | 50 | 80 | 100 | 100 |
| Fossil fuel $CO_2$ (excl. biofuels) | −1000 | −32 | −34 | 3 | 45 | 70 | 50 | 37 |
| Biofuel $CO_2$ | 90 | −27 | −28 | 30 | 5 | 10 | $\overline{m_{bf}} = 50$ | $\overline{m_{bf}} = 63$ |
| Fuel $CO_2$ excl. traffic $CO_2$ (but incl. biofuels) | −990 | −31.5 | −33.8 | 7 | 35 | 67 | 70 | 80 |
| Traffic fuel $CO_2$ | −1000 | −31 | −31 | 7 | 15 | 13 | $\overline{m_{tr}} = 30$ | $\overline{m_{tr}} = 20$ |
| Biospheric $CO_2$ | 60 | −23 | −25.5 | 0 | 50 | 20 | 0 | 0 |

nate from fuel emissions:

$$y_F = \Delta y, \tag{A1}$$

with $\Delta y = y_{tot} - y_{bg}$.

This simple approach is valid if (nearly) all $CO_2$ emissions are from fuel burning, as might be the case in cold winters or in areas without biospheric activity (e.g., megacities).

### A1.2 CO as a tracer for fuel $CO_2$

The CO offset ($\Delta x = x_{tot} - x'_{bg}$) can be used to estimate fuel $CO_2$ offset if it is divided by the mean ratio $\overline{R_F} = \Delta x / \Delta y_F$ of all fuel sources:

$$y_F = \frac{\Delta x}{\overline{R_F}}. \tag{A2}$$

Note that, in reality, the ratio $\overline{R_F}$ varies depending on the share of emissions of different emission sectors in the catchment area and their temporal emission patterns, as well as due to natural CO sources and sinks, at least in summer (Prather et al., 2001). We show $\overline{R_F}$ with an overbar to emphasize that this is a footprint-weighted average of the fuel emission ratio.

### A1.3 CO as a tracer for traffic $CO_2$ and $\delta^{13}C(CO_2)$ as a tracer for all fuel $CO_2$, except for traffic $CO_2$

We now include $\delta^{13}C(CO_2)$ in fuel $CO_2$ estimation as a tracer for all fuel $CO_2$ except those of traffic ($y_{F\text{-}tr} = y_{ff} + y_{bf} - y_{tr}$).

$$y_{tot} = y_{bg} + y_{bio} + y_{tr} + y_{F-tr} \tag{A3}$$

$$y_{tot}\delta_{tot} = y_{bg}\delta_{bg} + y_{bio}\delta_{bio} + y_{tr}\overline{\delta_{tr}} + y_{F-tr}\overline{\delta_{F\text{-}tr}} \tag{A4}$$

In analogy to $\overline{R_F}$ we show $\overline{\delta_{tr}}$ and $\overline{\delta_{F\text{-}tr}}$ with an overbar to emphasize that these are footprint-weighted averages of the emission groups traffic $CO_2$ and fuel $CO_2$ excluding traffic, respectively. Solving Eq. (A3) for $y_{bio}$, we can substitute $y_{bio}$ in Eq. (A4). In analogy to Eq. (A2), we use CO as a tracer for traffic $CO_2$:

$$y_{tr}(t) = \frac{x_{tr}(t)}{\overline{R_{tr}}}, \tag{A5}$$

with the mean $\Delta CO / \Delta CO_2$ ratio of traffic $\overline{R_{tr}} = (\Delta x / \Delta y)_{tr}$. $CO_{tr}$ can be determined from

$$CO_{tr}(t) = \Delta CO(t) \cdot \overline{m_{tr}}, \tag{A6}$$

with $\overline{m_{tr}} = (\Delta x_{tr} / \Delta x)$ being the share of traffic CO to the total CO offset. $\overline{m_{tr}}$ needs to be estimated from bottom-up inventories and can be found in Table A1 (right column) and is also dependent on the footprint area of the measurement site and the sources and sinks lying in this area. Equations (A3)–(A6) can then be rearranged:

$$y_{F-tr} = \frac{y_{tot}\delta_{tot} - y_{bg}\delta_{bg} - \left(y_{tot} - y_{bg} - y_{tr}\right)\delta_{bio} - y_{tr}\overline{\delta_{tr}}}{\overline{\delta_{F\text{-}tr}} - \delta_{bio}}. \tag{A7}$$

Total fuel $CO_2$ ($y_F$) contribution can then be determined as the sum of $y_{tr}$ (Eq. A5) and $y_{F\text{-}tr}$ (Eq. A7).

### A1.4 CO as a tracer for biofuel $CO_2$ and $\delta^{13}C(CO_2)$ as a tracer for all fuel $CO_2$, except for biofuel $CO_2$

This method of fuel $CO_2$ estimation is in analogy to case A.1.3, but instead of separating fuel $CO_2$ into traffic contributions ($y_{tr}$) and others ($y_{F\text{-}tr}$), we separate it into biofuel contributions ($y_{bf}$) and others ($y_{F\text{-}bf} = y_{ff}$); this leads to

$$y_{F-bf} = \frac{y_{tot}\delta_{tot} - y_{bg}\delta_{bg} - (y_{tot} - y_{bg} - y_{bf})\delta_{bio} - y_{bf}\overline{\delta_{bf}}}{\overline{\delta_{ff}} - \delta_{bio}}. \quad \text{(A8)}$$

Analogously to Eq. (A10), we formulate for $y_{bf}$:

$$y_{bf}(t) = \frac{\Delta x(t) \cdot \overline{m_{bf}}}{\overline{R_{bf}}}, \quad \text{(A9)}$$

with $\overline{m_{bf}} = (\Delta x_{bf}/\Delta x)$ from bottom-up inventories (see Table A1). Total fuel $CO_2$ ($y_F$) is calculated as the sum of $y_{bf}$ (Eq. A9) and $y_{F\text{-}bf}$ (Eq. A9).

### A1.5 $\delta^{13}C(CO_2)$ as the sole tracer for fuel emission

When using $\delta_{tot}$ as a tracer for all fuel contributions, Eq. (A3) and Eq. (A4) simplify to

$$y_F = \frac{y_{tot}\delta_{tot} - y_{bg}\delta_{bg} - (y_{tot} - y_{bg})\delta_{bio}}{\overline{\delta_F} - \delta_{bio}} \quad \text{(A10)}$$

if all fuel $CO_2$ ($y_{F\text{-}tr}$ and $y_{tr}$) contributions are pooled to $y_F$.

### A1.6 $\Delta^{14}C(CO_2)$ as a tracer for fossil fuel $CO_2$

Following Levin et al. (2008), we can derive fossil fuel $CO_2$ from $\Delta^{14}C(CO_2)$and total $CO_2$ measurements according to

$$y_{ff} = \frac{y_{bg}\left(\Delta^{14}C_{bg} - \Delta^{14}C_{bio}\right) - y_{tot}\left(\Delta^{14}C_{tot} - \Delta^{14}C_{bio}\right) - y_{bf}\left(\Delta^{14}C_{bio} - \Delta^{14}C_{bf}\right)}{1 + \Delta^{14}C_{bio}}. \quad \text{(A11)}$$

However, since $\Delta^{14}C_{bio} \approx \Delta^{14}C_{bf}$, and because biofuel contributions are not known, we neglect the last term of the numerator in the following. Note that, since $\Delta^{14}C(CO_2)$ is not sensitive to biofuel contributions, it is only possible to estimate the fossil fuel $CO_2$ contributions without biofuel contributions.

## A2 Determination of parameters and variables

The background values $y_{bg}$, $x'_{bg}$, $\delta_{bg}$ and $\Delta^{14}C_{bg}$ should represent the regional clean air to which the source contributions from the footprint area are added. Since there are often no nearby clean-air observations available for a polluted station, we use those mole fractions as a background where the air masses in the boundary layer are well mixed with the free troposphere. This is usually the case in the afternoon and is associated with low mole fractions. Since $CO_2$ and CO both have local sinks relevant on the timescale of days, we here use $CH_4$ as an indicator for a well-mixed boundary layer and assume that, when the $CH_4$ mole fraction reaches a minimum value (within 2 days), vertical mixing is strongest. In principal, if continuous radon measurements were available, these could also be used as an indicator for vertical mixing (Dörr et al., 1983), instead of $CH_4$. We checked that the $CH_4$ minimum values always represent a lower envelope of the simulated greenhouse gas record and does not vary at the synoptic timescale. We then use the total mole fractions and isotopic records $y_{tot}$, $x_{tot}$, $\delta_{tot}$, and $\Delta^{14}C_{tot}$ observed during situations with minimal $CH_4$ mole fractions as background values.

Further, in order to solve Eqs. (A2)–(A11), we need the input parameters $\delta_{bio}$ and $\Delta^{14}C_{bio}$. These input parameters were assigned with the objective of creating a realistic modeled data set (see Tables 1 and A1). Additionally, the integrated footprint-weighted parameters $\overline{R_F}$, $\overline{R_{tr}}$, $\overline{R_{bf}}$, $\overline{\delta_F}$, $\overline{\delta_{ff}}$, $\overline{\delta_{bf}}$, $\overline{\delta_{tr}}$, $\overline{\delta_{bio}}$, $\overline{\delta_{F\text{-}tr}}$, $\overline{m_{bf}}$ and $\overline{m_{tr}}$ are required (see Table A1). We call these parameters footprint-weighted since the ratios and isotopic signatures depend on the relative contribution from the different emission sectors (with their sector specific emission ratios and isotopic signatures) within the footprint of the measurement site. We represent the integrated footprint-weighted parameters with an overbar to draw attention to the fact that the parameters are averaged over the (e.g., monthly) footprint area. Even though the emission factors of the source categories used here are fixed for every pixel, integrated footprint-weighted $\overline{R_F}$, $\overline{R_{tr}}$, $\overline{R_{bf}}$, $\overline{\delta_F}$ $\overline{\delta_{ff}}$, $\overline{\delta_{bf}}$, $\overline{\delta_{tr}}$, $\overline{\delta_{bio}}$, $\overline{\delta_{F\text{-}tr}}$, $\overline{m_{bf}}$ and $\overline{m_{tr}}$ are not constant in time, because the footprint of the measurement site and the emission patterns are temporally variable. Thus, the footprint-weighted parameters change when the emissions from the different sectors or the footprint of the measurement site vary. Note that for our model study we do not require the parameters to be absolutely correct, since we do not compare them to measured data. However, since we want to provide a realistic case study, we seek to use the most realistic parameters (see values in Tables 1 and A1).

## Appendix B: "Calibration" with $\Delta^{14}C(CO_2)$

Solving Eqs. (A3), (A8), (A9) and (A11) for fuel $CO_2$ requires $\overline{R_F}$, $\overline{\delta_F}$, $\overline{\delta_{ff}}$ and $\overline{\delta_{F\text{-}tr}}$. If these values are not known, they may be derived from $\Delta^{14}C(CO_2)$observations (what we then call $\Delta^{14}C(CO_2)$-calibrated). For the calibration, $y_{ff}$ must be known. The idea is to calibrate fossil fuel $CO_2$, e.g., with precise $\Delta^{14}C(CO_2)$measurements, on a lower time resolution (e.g., monthly) and assume that the footprint-weighted parameters $\overline{R_F}$, $\overline{\delta_F}$, $\overline{\delta_{ff}}$ and $\overline{\delta_{F\text{-}tr}}$ do not change significantly within this calibration interval.

Re-arranging Eqs. (1) and (2) for $\overline{\delta_{ff}}$ leads to

$$\overline{\delta_{ff}} = \frac{y_{tot}\delta_{tot} - y_{bg}\delta_{bg} - (y_{tot} - y_{bg} - y_{ff} - y_{bf})\delta_{bio} - y_{bf}\overline{\delta_{bf}}}{y_{ff}}, \quad \text{(B1)}$$

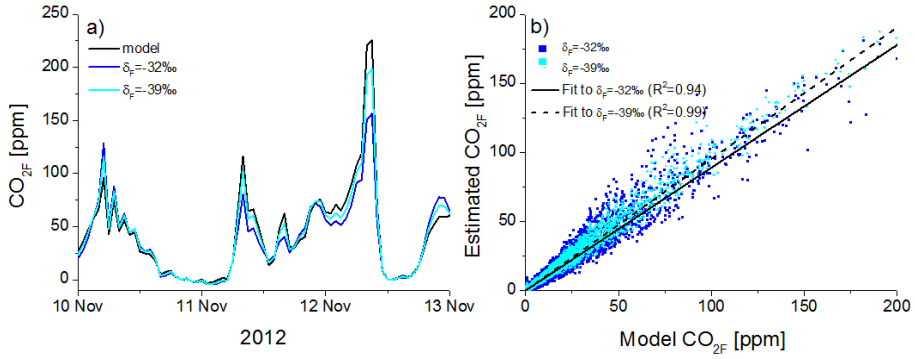


**Figure B1. (a)** Example period showing fuel $CO_2$ of different fuel $CO_2$ estimation methods and reference modeled fuel $CO_2$. Dark blue: mean $\delta_F$ is $-32$ ‰; cyan: mean $\delta_F$ is $-39$ ‰. **(b)** Correlation plot between estimated and modeled fuel $CO_2$ for mean $\delta_F = -32$ ‰ (dark blue and solid line) and mean $\delta_F = -39$ ‰ (cyan and dotted line) during the entire year of 2012. Fuel $CO_2$ can be estimated much better using $\delta^{13}C(CO_2)$ when the fuel $\delta^{13}C$ signature is strongly depleted with respect to the biosphere. Note that the slope slightly changes when using more depleted sources. This is because few high fuel $CO_2$ peaks span the linear regression and therefore determine the slope to a large degree, but as a general tendency for the Heidelberg data set, the high fuel $CO_2$ peaks exhibit an isotopic signature, which is more enriched as the isotopic signature of the mean fuel source mix.

which could then be used in Eq. (A9). Note that we require the biofuel $CO_2$ in addition to the fossil fuel $CO_2$ from $\Delta^{14}C(CO_2)$.

$\overline{\delta_F}$ can then be derived if the $y_{bf}$ concentration is known.

$$\overline{\delta_F} = \frac{\overline{\delta_{ff}} y_{ff} + \overline{\delta_{bf}} y_{bf}}{y_{ff} + y_{bf}} \tag{B2}$$

If fossil fuel emissions are divided into fossil fuel contributions without traffic ($y_{F\text{-}tr}$) and traffic contributions ($y_{tr}$), we can derive $\overline{\delta_{F\text{-}tr}}$ required for solving Eq. (A8):

$$\overline{\delta_{F\text{-}tr}} = \frac{\overline{\delta_F} y_F - \overline{\delta_{tr}} y_{tr}}{y_F - y_{tr}}. \tag{B3}$$

Analogously, the ratio $\overline{R_F}$ could be calibrated following

$$\overline{R_F} = \frac{\Delta x}{\Delta y_F}. \tag{B4}$$

In order to calculate the monthly mean value of $\langle\overline{\delta_F}\rangle$ and $\langle\overline{R_F}\rangle$, the mean ratios $\langle\frac{\Delta x}{\Delta y_F}\rangle$ (Eqs. B1–B4) are needed. However, from integrated $\Delta^{14}C(CO_2)$ sampling, we only have the mean fossil fuel $CO_2$ and fuel $CO_2$ values and can thus only calculate $\langle\Delta x\rangle/\langle\Delta y_F\rangle$. Using the product (or ratio) of the means rather than the mean of the product (ratio) is only correct if the factors are uncorrelated. Since the factors in Eqs. (B1)–(B4) (and $\Delta x$ and $\Delta y_{ff}$) are correlated, the integrated calibration cannot be applied without introducing a bias into monthly mean $\langle\overline{\delta_F}\rangle$, $\langle\overline{\delta_{ff}}\rangle$, $\langle\overline{\delta_{F\text{-}tr}}\rangle$ and $\langle\overline{R_F}\rangle$. Instead of using integrated $\Delta^{14}C(CO_2)$ samples in order to obtain the monthly fossil fuel $CO_2$ values, it is possible to take grab samples and analyze these for $\Delta^{14}C(CO_2)$ (and with that $y_{ff}$), total $CO_2$, $\delta^{13}C(CO_2)_{tot}$ and CO in order to calculate the individual (non-averaged) values for $\overline{\delta_F}$, $\overline{\delta_{F\text{-}tr}}$, $\overline{\delta_{ff}}$ and $\overline{R_F}$ (see Sect. 4).

## Appendix C: Influence of more depleted fuel $\delta^{13}C(CO_2)$ signatures

We have argued that we only require a realistic set of input parameters, rather than an absolutely correct set of parameters to estimate uncertainties of the different tracer methods. However, the results presented so far are to some degree dependent on the emission characteristics used in our model (see Table A1). When using CO as a tracer for fuel $CO_2$, it would be advantageous if natural sources of CO were negligible and if the emission ratio $\overline{R_F}$ were the same for all sources. When using $CO_2$ as a tracer for fuel $CO_2$, biospheric $CO_2$ emissions should be negligible, and when using $\delta^{13}C(CO_2)$, it would be advantageous if fuel $CO_2$ emissions were strongly depleted compared to biospheric emissions. It is beyond the scope of this work to show explicitly, for all cases, how the "choice" of different emission characteristics influences the fuel $CO_2$ estimate in terms of precision and accuracy. However, in Fig. B1, we illustrate for this latter case how the presence of more depleted fuel sources in the footprint area of the measurement site could improve the tracer $\delta^{13}C(CO_2)$ for fuel $CO_2$ estimation. This should serve as an example showing how much the emission characteristics at a site may influence the precision of fuel $CO_2$ estimates using different tracer configurations.

Figure B1 shows that fuel $CO_2$ can be estimated much better when the mean source mix in the catchment area of the measurement site exhibits a strongly depleted isotopic source signature. The regression coefficient improves from 0.94 to 0.99 and the precision within 1 year decreases significantly by 40 % when choosing $\overline{\delta_F}$ that is 7 ‰ more depleted ($-39$ ‰ instead of $-32$ ‰). The precision of $\delta^{13}C(CO_2)$-based fuel $CO_2$ will increase with decreasing isotopic signature of fuel $CO_2$ sources. Analogously, the precision of CO-based fuel

$CO_2$ estimates will increase with decreasing inhomogeneity of $CO / CO_2$ ratio of fuel $CO_2$ sources. This effect should be taken into account when designing a measurement network and thus highlights the importance of a thorough source evaluation in the catchment area prior to instrumental installation.

## Appendix D: List of abbreviations

| | |
|---|---|
| AMS | Accelerator mass spectrometry |
| bf | Biofuel |
| bg | Background |
| bio | Biosphere |
| EDGAR | Emissions Database for Global Atmospheric Research |
| F | Fuel |
| F-bf | Fuel excluding biofuels (i.e., ff) |
| ff | Fossil fuel |
| F-tr | Fuel excluding traffic |
| GC | Gas chromatography |
| ICOS | Integrated Carbon Observation System |
| IQR | Interquartile range |
| $m_x$ | CO share of emission group $x$ to CO offset |
| NPP | Nuclear power plant |
| ppm | parts per million, equivalent to $\mu$mol mol$^{-1}$ |
| $R_x$ | Ratio of CO to $CO_2$ in the emission group $x$ |
| SD | Standard deviation |
| STILT | Stochastic Time-Inverted Lagrangian Particle model |
| tot | Total |
| $x$ | CO mole fraction |
| $y$ | $CO_2$ mole fraction |

*Acknowledgements.* We thank Ute Karstens and Thomas Koch for valuable modeling lessons and help with setting up the model. We are also grateful for valuable discussions on fossil fuel $CO_2$ in Heidelberg with Felix R. Vogel and Samuel Hammer. We would also like to thank Jocelyn Turnbull and the anonymous referee for their valuable feedback. This work has been funded by the InGOS EU project (284274) and ICOS BMBF project (01LK1225A). Further, we acknowledge the financial support given by Deutsche Forschungsgemeinschaft and Ruprecht-Karls-Universität Heidelberg within the funding program Open Access Publishing.

Edited by: J. Kaiser

## References

Andres, R. J., Marland, G., Boden, T., and Bischof, S.: Carbon dioxide emissions from fossil fuel consumption and cement manufacture, 1751–1991; and an estimate of their isotopic composition and latitudinal distribution (No. CONF-9307181–4). Oak Ridge National Lab., TN (United States); Oak Ridge Inst. for Science and Education, TN (United States), 1994.

Atkinson, R.: Atmospheric chemistry of VOCs and $NO_x$, Atmos. Environ., 34, 2063–2101, 2000.

Ballantyne, A. P., Miller, J. B., Baker, I. T., Tans, P. P., and White, J. W. C.: Novel applications of carbon isotopes in atmospheric $CO_2$: what can atmospheric measurements teach us about processes in the biosphere?, Biogeosciences, 8, 3093–3106, doi:10.5194/bg-8-3093-2011, 2011.

Bousquet, P., Peylin, P., Ciais, P., Le Quéré, C., Friedlingstein, P., and Tans, P. P.: Regional changes in carbon dioxide fluxes of land and oceans since 1980, Science, 290, 1342–1346, 2000.

BP: The role of biofuels beyond 2020, Technical report issued September 2013, available at: http://www.bp.com/en/global/alternative-energy/our-businesses/biofuels.html, last access: February 2015.

Conrad, R.: Soil microorganisms as controllers of atmospheric trace gases ($H_2$, CO, $CH_4$, OCS, $N_2O$, and NO), Microbiol. Rev., 60, 609–640, 1996.

Coyle, W.: The future of biofuels, Economic Research Service, Washington, DC, 2007.

Denier van der Gon, H. D., Hendriks, C., Kuenen, J., Segers, A., and Visschedijk, A.: Description of current temporal emission patterns and sensitivity of predicted AQ for temporal emission patterns, TNP Report, EU FP7 MACC deliverable report D_D-EMIS_1.3, available at: https://gmes-atmosphere.eu/documents/deliverables/d-emis/MACC_TNO_del_1_3_v2.pdf, 2011.

Djuricin, S., Pataki, D. E., and Xu, X.: A comparison of tracer methods for quantifying $CO_2$ sources in an urban region, J. Geophys. Res., 115, D11303, doi:10.1029/2009JD012236, 2010.

Dörr, H., Kromer, B., Levin, I., Münnic, K. O., and Volpp, H.-J.: $CO_2$ and radon 222 as tracers for atmospheric transport, J. Geophys. Res., 88, 1309–1313, doi:10.1029/JC088iC02p01309, 1983.

Esler, M. B., Griffith, D. W. T., Wilson, S. R., and Steele, L. P.: Precision trace gas analysis by FT-IR spectroscopy. 2. The $^{13}C/^{12}C$ isotope ratio of $CO_2$, Anal. Chem, 72.1, 216–221, 2000.

EC-JRC/PBL European Commission – Joint Research Centre/PBL Netherlands Environmental Assessment Agency, The Emissions Database for Global Atmospheric Research (EDGAR) version 4.3, available at: http://edgar.jrc.ec.europa.eu/, 2015.

Flanagan, L. B., Ehleringer, J. R., and Pataki D. E. (Eds.): Stable isotopes and biosphere-atmosphere interactions, Elsevier Academic Press, San Diego, US, 318 pp., 2005.

Galli, I., Bartalini, S., Cancio, P., De Natale, P., Mazzotti, D., Giusfredi, G., Fedi, M. E., and Mando, P. A.: Optical detection of radiocarbon dioxide: first results and AMS intercomparison, Radiocarbon, 55, 213–223, 2013.

Gamnitzer, U., Karstens, U., Kromer, B., Neubert, R. E., Meijer, H. A., Schroeder, H., and Levin, I.: Carbon monoxide: A quantitative tracer for fossil fuel $CO_2$?, J. Geophys. Res.-Atmos., 111, 2156–2202, doi:10.1029/2005JD006966, 2006.

Gerbig, C., Lin, J. C., Wofsy, S. C., Daube, B. C., Andrews, A. E., Stephens, B. B., Bakwin, P. S., and Grainger, C. A.: Toward constraining regional-scale fluxes of $CO_2$ with atmospheric observations over a continent: 2. Analysis of COBRA data using a receptor-oriented framework, J. Geophys. Res.-Atmos., 108, 4756, doi:10.1029/2003JD003770, 2003.

Gerbig, C., Körner, S., and Lin, J. C.: Vertical mixing in atmospheric tracer transport models: error characterization and propagation, Atmos. Chem. Phys., 8, 591–602, doi:10.5194/acp-8-591-2008, 2008.

Granier, C., Pétron, G., Müller, J.-F., and Brasseur, G.: The impact of natural and anthropogenic hydrocarbons on the tropospheric budget of carbon monoxide, Atmos. Environ., 34, 5255–5270, 2000.

Graven, H. D. and Gruber, N.: Continental-scale enrichment of atmospheric $^{14}CO_2$ from the nuclear power industry: potential impact on the estimation of fossil fuel-derived $CO_2$, Atmos. Chem. Phys., 11, 12339–12349, doi:10.5194/acp-11-12339-2011, 2011.

Gros, V., Tsigaridis, K., Bonsang, B., Kanakidou, M., and Pio, C.: Factors controlling the diurnal variation of CO above a forested area in southeast Europe, Atmos. Environ., 36, 3127–3135, 2002.

Gurney, K. R., Law, R. M., Denning, A. S., Rayner, P. J., Baker, D., Bousquet, P., Bruhwiler, L., Chen, Y., Ciais, C., Fan, S., Fung, I. Y., Gloor, M., Heimann, M., Higuchi, John,J., Maki, T., Maksyutov, S., Masarie, K., Peylin, P., Prather, M., Pak, B. C., Randerson, J., Sarmiento, J., Taguc, S., Takahashi, T., and Yuen, C. W.: Towards robust regional estimates of $CO_2$ sources and sinks using atmospheric transport models, Nature, 415, 626–630, 2002.

Gurney, K. R., Chen, Y.-H., Maki, T., Kawa, S. R., Andrews, A., and Zhu, Z.: Sensitivity of atmospheric $CO_2$ inversions to seasonal and interannual variations in fossil fuel emissions, J. Geophys. Res., 110, D10308, doi:10.1029/2004JD005373, 2005.

Hammer, S., Griffith, D. W. T., Konrad, G., Vardag, S., Caldow, C., and Levin, I.: Assessment of a multi-species in situ FTIR for precise atmospheric greenhouse gas observations, Atmos. Meas. Tech., 6, 1153–1170, doi:10.5194/amt-6-1153-2013, 2013.

Heimann, M. and Koerner, S.: The global atmospheric tracer model TM3, Technical Reports, Max-Planck-Institute for Biogeochemie, 5, 131 pp., 2003.

IEA, International Energy Agency: Key World Energy Statistics 2014, available at: http://www.iea.org/publications/freepublications/publication/key-world-energy-statistics-2014.html (last access: 30 September 2015), 2014.

Inman, R. E., Ingersoll, R. B., and Levy, E. A.: Soil: A natural sink for carbon monoxide, Science, 172, 1229–1231, doi:10.1126/science.172.3989.1229, 1971.

Jung, M., Henkel, K., Herold, M., and Churkina, G.: Exploiting synergies of global land cover products for carbon cycle modeling, Remote Sens. Environ., 101, 534–553, 2006.

Kaul, M.: Isotopenverhältnisse im atmosphärischem Kohlendioxid und seine Quellen im Raum Heidelberg, Staatsexamensarbeit, 2007.

Keeling, C. D.: The concentration and isotopic abundances of atmospheric carbon dioxide in rural areas, Geochim. Cosmochim. Acta, 13, 322–334, 1958.

Keeling, C. D.: The concentration and isotopic abundances of carbon dioxide in the atmosphere, Tellus, 12.2, 200–203, 1960.

Keeling, C. D.: The concentration and isotopic abundance of carbon dioxide in rural and marine air, Geochim. Cosmochim. Acta, 24, 277–298, 1961.

Keeling, R. F., Piper, S. C., and Heimann, M.: Global and hemispheric $CO_2$ sinks deduced from changes in atmospheric $O_2$ concentration, Nature, 381, 218–221, 1996.

Le Quéré, C., Moriarty, R., Andrew, R. M., Peters, G. P., Ciais, P., Friedlingstein, P., Jones, S. D., Sitch, S., Tans, P., Arneth, A., Boden, T. A., Bopp, L., Bozec, Y., Canadell, J. G., Chini, L. P., Chevallier, F., Cosca, C. E., Harris, I., Hoppema, M., Houghton, R. A., House, J. I., Jain, A. K., Johannessen, T., Kato, E., Keeling, R. F., Kitidis, V., Klein Goldewijk, K., Koven, C., Landa, C. S., Landschützer, P., Lenton, A., Lima, I. D., Marland, G., Mathis, J. T., Metzl, N., Nojiri, Y., Olsen, A., Ono, T., Peng, S., Peters, W., Pfeil, B., Poulter, B., Raupach, M. R., Regnier, P., Rödenbeck, C., Saito, S., Salisbury, J. E., Schuster, U., Schwinger, J., Séférian, R., Segschneider, J., Steinhoff, T., Stocker, B. D., Sutton, A. J., Takahashi, T., Tilbrook, B., van der Werf, G. R., Viovy, N., Wang, Y.-P., Wanninkhof, R., Wiltshire, A., and Zeng, N.: Global carbon budget 2014, Earth Syst. Sci. Data, 7, 47–85, doi:10.5194/essd-7-47-2015, 2015.

Levin, I. and Karstens, U.: Inferring high-resolution fossil fuel $CO_2$ records at continental sites from combined ($CO_2$)-C-14 and CO observations, Tellus B, 59, 245–250, doi:10.1111/j.1600-0889.2006.00244.x, 2007.

Levin, I., Kromer, B., Schmidt, M., and Sartorius, H.: A novel approach for independent budgeting of fossil fuel $CO_2$ over Europe by $^{14}CO_2$ observations, Geophys. Res. Lett., 30, 2194, doi:10.1029/2003GL018477, 2003.

Levin, I., Hammer, S., Kromer, B., and Meinhardt, F.: Radiocarbon observations in atmospheric $CO_2$: Determining fossil fuel $CO_2$ over Europe using Jungfraujoch observations as background, Sci. Total Environ., 391, 211–216, 2008.

Lin, J. C., Gerbig, C., Wofsy, S. C., Andrews, A. E., Daube, B. C., Davis, K. J., and Grainger, C. A.: A near-field tool for simulating the upstream influence of atmospheric observations: The Stochastic Time-Inverted Lagrangian Transport (STILT) model, J. Geophys. Res., 108, 4493, doi:10.1029/2002JD003161, 2003.

Mahadevan, P., Wofsy, S. C., Matross, D. M., Xiao, X., Dunn, A. L., Lin, J. C., Gerbig, C., Munger, J. W., Chow, V. Y., and Gottlieb, E. W.: A satellite-based biosphere parameterization for net ecosystem $CO_2$ exchange: Vegetation Photosynthesis and Respiration Model (VPRM), Global Biogeochem. Cy., 22, GB2005, doi:10.1029/2006GB002735, 2008.

McIntyre, C. P., McNicholm, A. P., Roberts, M. L., Seewald, J. S., von Reden, K. F., and Jenkins, W. J.: Improved Precision of $^{14}C$ Measurements for $CH_4$ and $CO_2$ Using GC and Continuous-Flow AMS Achieved by Summation of Repeated Injections, Radiocarbon, 55, 677–685, 2013.

Meijer, H. A. J., Smid, H. M., Perez, E., and Keizer, M. G.: Isotopic characterization of anthropogenic $CO_2$ emissions using isotopic and radiocarbon analysis, Phys. Chem. Earth, 21, 483–487, 1996.

Mook, W. M. E.: Environmental Isotopes in the Hydrological Cycle. Principles and Applications, UNESCO/IAEA Series, http://www-naweb.iaea.org/napc/ih/documents/global_cycle/Environmental%20Isotopes%20in%20the%20Hydrological%20Cycle%20Vol%201.pdf, 2001.

Newman, S., Jeong, S., Fischer, M. L., Xu, X., Haman, C. L., Lefer, B., Alvarez, S., Rappenglueck, B., Kort, E. A., Andrews, A. E., Peischl, J., Gurney, K. R., Miller, C. E., and Yung, Y. L.: Diurnal tracking of anthropogenic $CO_2$ emissions in the Los Angeles basin megacity during spring 2010, Atmos. Chem. Phys., 13, 4359–4372, doi:10.5194/acp-13-4359-2013, 2013.

Newman, S., Xu, X., Gurney, K. R., Hsu, Y.-K., Li, K.-F., Jiang, X., Keeling, R., Feng, S., O'Keefe, D., Patarasuk, R., Wong, K. W., Rao, P., Fischer, M. L., and Yung, Y. L.: Toward consis-

tency between bottom-up CO2 emissions trends and top-down atmospheric measurements in the Los Angeles megacity, Atmos. Chem. Phys. Discuss., 15, 29591–29638, doi:10.5194/acpd-15-29591-2015, 2015.

Parrish, D. D., Trainer, M., Holloway, J. S., Yee, J., Warshawsky, S., Fehsenfeld, F., Forbes,G., and Moody, J.: Relationships between ozone and carbon monoxide at surface sites in the North Atlantic region, J. Geophys. Res., 103, 13357–13376, doi:10.1029/98JD00376, 1993.

Pataki, D. E., Ehleringer, J. R., Flanagan, L. B., Yakir, D., Bowling, D. R., Still, C. J., Buchmann, N., Kaplan, J. O., and Berry, J. A.: The application and interpretation of Keeling plots in terrestrial carbon cycle research, Global Biogeochem. Cy., 17, 1022, doi:10.1029/2001GB001850, 2003.

Pataki, D. E., Alig, R. J., Fung, A. S., Golubiewski, N. E., Kennedy, C. A., McPherson, E. G., Nowak, D. J., Pouyat, R. V., and Romero Lankao, P.: Urban ecosystems and the North American carbon cycle, Global Change Biol., 12, 2092–2102, doi:10.1111/j.1365-2486.2006.01242.x, 2006.

Peylin, P., Houweling, S., Krol, M. C., Karstens, U., Rödenbeck, C., Geels, C., Vermeulen, A., Badawy, B., Aulagnier, C., Pregger, T., Delage, F., Pieterse, G., Ciais, P., and Heimann, M.: Importance of fossil fuel emission uncertainties over Europe for $CO_2$ modeling: model intercomparison, Atmos. Chem. Phys., 11, 6607–6622, doi:10.5194/acp-11-6607-2011, 2011.

Peylin, P., Law, R. M., Gurney, K. R., Chevallier, F., Jacobson, A. R., Maki, T., Niwa, Y., Patra, P. K., Peters, W., Rayner, P. J., Rödenbeck, C., van der Laan-Luijkx, I. T., and Zhang, X.: Global atmospheric carbon budget: results from an ensemble of atmospheric $CO_2$ inversions, Biogeosciences, 10, 6699–6720, doi:10.5194/bg-10-6699-2013, 2013.

Prather, M., Ehhalt, D., Dentener, F., Derwent, R. G., Dlugokencky, E., Holland, E., Isaksen, I. S. A., Katima, J., Kirchhoff, V., Matson, P., Midgley, P. M., and Wang, M.: Atmospheric chemistry and greenhouse gases, in: Climate Change 2001, edited by: Houghton, J. T., 239–287, Cambridge Univ. Press, New York, 2001.

Rödenbeck, C.: Estimating $CO_2$ sources and sinksfrom atmospheric mixing ratio measurements using a global inversion of atmospheric transport, Max Planck Institute for Biogeochemistry, Jena, Germany, available at: http://www.bgc-jena.mpg.de/bgc-systems/pmwiki2/uploads/Publications/6.pdf, 2005.

Rogelj, J., McCollum, D., Smith, S., Calvin, K., Clarke, L., Garg, A., Jiang, K., Krey, V., Lowe, J., Riahi, K., Schaeffer, M., van Vuuren, D., Wenying, C., Crippa, M., and Janssens-Maenhout, G.: Chapter 2 of The emission gap report 2014: What emission levels will comply with temperature limit. In: The emission gap report 2014: a UNEP synthesis report, United Nations Environment Programme (UNEP), 2014.

Rivier, L., Ciais, P., Hauglustaine, D. A., Bakwin, P., Bousquet, P, Peylin, P., and Klonecki, A.: Evaluation of $SF_6$, $C_2Cl_4$ and CO to approximate fossil fuel $CO_2$ in the Northern Hemisphere using a chemistry transport model, J. Geophys. Res., 111, D16311, doi:10.1029/2005JD006725, 2006.

Schmidt, A., Rella, C. W., Göckede, M., Hanson, C., Yang, Z., and Law, B. E.: Removing traffic emissions from $CO_2$ time series measured at a tall tower using mobile measurements and transport modeling, Atmos. Environ., 97, 94–108, doi:10.1016/j.atmosenv.2014.08.006, 2014.

Steinbach, J., Gerbig, C., Rödenbeck, C., Karstens, U., Minejima, C., and Mukai, H.: The $CO_2$ release and Oxygen uptake from Fossil Fuel Emission Estimate (COFFEE) dataset: effects from varying oxidative ratios, Atmos. Chem. Phys., 11, 6855–6870, doi:10.5194/acp-11-6855-2011, 2011.

Stuiver, M. and Polach, H. A.: Reporting of C-14 data-Discussion, Radiocarbon, 19, 355–363, 1977.

Taylor, A. J., Lai, C. T., Hopkins, F. M., Wharton, S., Bible, K., Xu, X., Philipps, C., Bush, S., and Ehleringer, J. R.: Radiocarbon-Based Partitioning of Soil Respiration in an Old-Growth Coniferous Forest, Ecosystems, 18, 1–12, 2015.

Trusilova, K., Rödenbeck, C., Gerbig, C., and Heimann, M.: Technical Note: A new coupled system for global-to-regional downscaling of $CO_2$ concentration estimation, Atmos. Chem. Phys., 10, 3205–3213, doi:10.5194/acp-10-3205-2010, 2010.

Turnbull, J. C., Miller, J. B., Lehman, S. J., Tans, P. P., Sparks, R. J., and Southon, J.: Comparison of $^{14}CO_2$, CO, and $SF_6$ as tracers for recently added fossil fuel $CO_2$ in the atmosphere and implications for biological $CO_2$ exchange. Geophys. Res. Lett., 33, L01817, doi:10.1029/2005GL024213, 2006.

Turnbull, J. C., Lehman, S. J., Miller, J. B., Sparks, R. J., Southon, J. R., and Tans, P. P.: A new high precision $^{14}CO_2$ time series for North American continental air, J. Geophys. Res., 112, D11310, doi:10.1029/2006JD008184, 2007.

Turnbull, J. C., Karion, A., Fischer, M. L., Faloona, I., Guilderson, T., Lehman, S. J., Miller, B. R., Miller, J. B., Montzka, S., Sherwood, T., Saripalli, S., Sweeney, C., and Tans, P. P.: Assessment of fossil fuel carbon dioxide and other anthropogenic trace gas emissions from airborne measurements over Sacramento, California in spring 2009, Atmos. Chem. Phys., 11, 705–721, doi:10.5194/acp-11-705-2011, 2011.

Turnbull, J. C., Sweeney, C., Karion, A., Newberger, T., Lehman, S. J., Tans, P. P., Davis, K. J., Lauvaux, T., Miles, N. L., Richardson, S. J., Cambaliza, M. O., Shepson, P. B., Gurney, K., Patarasuk, R., and Razlivanov, I.: Toward quantification and source sector identification of fossil fuel $CO_2$ emissions from an urban area: Results from the INFLUX experiment, J. Geophys. Res.-Atmos., 120, 292–312, 2015.

Tuzson, B., Henne, S., Brunner, D., Steinbacher, M., Mohn, J., Buchmann, B., and Emmenegger, L.: Continuous isotopic composition measurements of tropospheric $CO_2$ at Jungfraujoch (3580 m a.s.l.), Switzerland: real-time observation of regional pollution events, Atmos. Chem. Phys., 11, 1685–1696, doi:10.5194/acp-11-1685-2011, 2011.

Vardag, S. N., Hammer, S., O'Doherty, S., Spain, T. G., Wastine, B., Jordan, A., and Levin, I.: Comparisons of continuous atmospheric $CH_4$, $CO_2$ and $N_2O$ measurements – results from a travelling instrument campaign at Mace Head, Atmos. Chem. Phys., 14, 8403–8418, doi:10.5194/acp-14-8403-2014, 2014.

Vardag, S. N., Hammer, S., Sabasch, M., Griffith, D. W. T., and Levin, I.: First continuous measurements of $\delta^{18}$O-$CO_2$ in air with a Fourier transform infrared spectrometer, Atmos. Meas. Tech., 8, 579–592, doi:10.5194/amt-8-579-2015, 2015.

Vogel, F. R.: $^{14}CO_2$-calibrated carbon monoxide as proxy to estimate the regional fossil fuel $CO_2$ component at hourly resolution, PhD thesis, Ruprecht-Karls University Heidelberg, Germany, 2010.

Vogel, F., Hammer, S., Steinhof, A., Kromer, B., and Levin, I.: Implication of weekly and diurnal $^{14}C$ calibration on

hourly estimates of CO-based fossil fuel $CO_2$ at a moderately polluted site in southwestern Germany, Tellus B, 62, doi:10.3402/tellusb.v62i5.16600, 2010.

Vogel, F. R., Huang, L., Ernst, D., Giroux, L., Racki, S., and Worthy, D. E. J.: Evaluation of a cavity ring-down spectrometer for in situ observations of $^{13}CO_2$, Atmos. Meas. Tech., 6, 301–308, doi:10.5194/amt-6-301-2013, 2013a.

Vogel, F., Levin, I., and Worthy, D.: Implications for Deriving Regional Fossil Fuel $CO_2$ Estimates from Atmospheric Observations in a Hot Spot of Nuclear Power Plant $^{14}CO_2$ Emissions, Radiocarbon, North America, 55, May 2013b.

Wang, R., Tao, S., Ciais, P., Shen, H. Z., Huang, Y., Chen, H., Shen, G. F., Wang, B., Li, W., Zhang, Y. Y., Lu, Y., Zhu, D., Chen, Y. C., Liu, X. P., Wang, W. T., Wang, X. L., Liu, W. X., Li, B. G., and Piao, S. L.: High-resolution mapping of combustion processes and implications for $CO_2$ emissions, Atmos. Chem. Phys., 13, 5189–5203, doi:10.5194/acp-13-5189-2013, 2013.

Widory, D., Proust, E., Bellenfant, G., and Bour, O.: Assessing methane oxidation under landfill covers and its contribution to the above atmospheric $CO_2$ levels: The added value of the isotope ($\delta^{13}$C and $\delta^{18}$O CO2; $\delta^{13}$C and $\delta$D $CH_4$) approach, Waste Manage, 32, 1685–1692, 2012.

Zondervan, A. and Meijer, H. A. J.: Isotopic characterisation of $CO_2$ sources during regional pollution events using isotopic and radiocarbon analysis, Tellus B, 48, 601–612, doi:10.1034/j.1600-0889.1996.00013.x, 1996.